Non-invasive stimulation of the human striatum disrupts reinforcement learning of motor skills

Pierre Vassiliadis[1,2,3] , Elena Beanato[1,2], Traian Popa[1,2], Fabienne Windel[1,2], Takuya Morishita[1,2], Esra Neufeld[4], Julie Duque[3], Gerard Derosiere[3,5], Maximilian J. Wessel[1,2,6] and Friedhelm C. Hummel[1,2,7 *]

[1]Defitech Chair of Clinical Neuroengineering, Neuro-X Institute (INX) and Brain Mind Institute (BMI), École Polytechnique Fédérale de Lausanne (EPFL), 1202 Geneva, Switzerland.

[2]Defitech Chair of Clinical Neuroengineering, INX and BMI, EPFL Valais, Clinique Romande de Réadaptation,1951 Sion, Switzerland.

[3]Institute of Neuroscience, Université Catholique de Louvain, 1200, Brussels, Belgium

[4]Foundation for Research on Information Technologies in Society, Zurich, Switzerland

[5]Lyon Neuroscience Research Center – Impact team - Inserm U1028 – CNRS UMR5292, Lyon 1 University, Bron, France

[6]Department of Neurology, University Hospital, Julius-Maximilians-University, Würzburg, Germany

[7]Clinical Neuroscience, University of Geneva Medical School, 1202 Geneva, Switzerland.

*** CORRESPONDENCE TO:**

Friedhelm C. Hummel

Neuro-X Institute (INX)

École Polytechnique Fédérale de Lausanne (EPFL)

Campus Biotech, Room H4.3.132.084

Chemin des Mines 9, 1202 Geneva, Switzerland

and

EPFL Valais,

Clinique Romande de Réadaptation

Av. Grand-Champsec 90,

CH-1951 Sion

Email: friedhelm.hummel@epfl.ch

Abstract

Reinforcement feedback can improve motor learning, but the underlying brain mechanisms remain unexplored. Especially, the causal contribution of specific patterns of oscillatory activity within the human striatum is unknown. To address this question, we exploited an innovative, non-invasive deep brain stimulation technique called transcranial temporal interference stimulation (tTIS) during reinforcement motor learning with concurrent neuroimaging, in a randomised, sham-controlled, double-blind study. Striatal tTIS applied at 80Hz, but not at 20Hz, abolished the benefits of reinforcement on motor learning. This effect was related to a selective modulation of neural activity within the striatum. Moreover, 80Hz, but not 20Hz, tTIS increased the neuromodulatory influence of the striatum on frontal areas involved in reinforcement motor learning. These results show for the first time that tTIS can non-invasively and selectively modulate a striatal mechanism involved in reinforcement learning, opening new horizons for the study of causal relationships between deep brain structures and human behaviour.

46 **Keywords:**

47 Motor learning, reward, reinforcement learning, non-invasive brain stimulation, deep brain

48 stimulation, temporal interference stimulation, striatum, neuroimaging

1. Introduction

The ability to learn from past outcomes, often referred to as reinforcement learning, is fundamental for biological systems[1]. Reinforcement learning has been classically studied in the context of decision making, when agents have to decide between a discrete number of potential options[2]. Importantly, there is an increasing recognition that reinforcement learning processes are also at play in other contexts including when one has to learn a new motor skill[3–5]. For instance, the addition of reinforcement feedback during motor training can improve motor learning, presumably by boosting the retention of newly acquired motor memories[6,7]. Interestingly, reinforcement feedback also appears to be relevant for the rehabilitation of patients suffering from motor impairments[8–10]. Yet, despite these promising results, there is currently a lack of understanding of the brain mechanisms that are critical to implement this behaviour.

A prominent hypothesis in the field is that the striatum, an area that is active both during reinforcement[11] and motor learning[12], may be causally involved in the beneficial effects of reinforcement on motor learning. As such, the striatum shares dense connexions with dopaminergic structures of the midbrain as well as with pre-frontal and motor cortical regions[13], and is therefore well positioned to translate information about reinforcement into motor adjustments[14–16]. This idea is in line with neuroimaging studies showing reward-related activation of the striatum during motor learning[17,18]. More specifically, within the striatum, oscillatory activity in specific frequency bands is suggested to be involved in aspects of reinforcement processing. As such, previous rodent studies have shown that striatal high gamma oscillations (~ 80 Hz) are sensitive to reward and dopamine and are highly coherent with the frontal cortex, suggesting that they may be involved in reinforcement learning[19–23]. In particular, dynamic changes of high gamma activity in the striatum[19,24,25] and in other parts of the basal ganglia[26,27] seem to encode the outcome of previous movements (i.e., success or failure). Hence, this body of work suggests that the fine-tuning of striatal oscillatory activity, especially in the gamma range, may be crucial for

reinforcement learning of motor skills. Conversely, striatal beta oscillations (~20 Hz) have been largely associated with sensorimotor functions[28]. For instance, beta oscillations in the striatum are exacerbated in Parkinson's disease and associated to the severity of motor symptoms[29–31]. Taken together, these elements suggest that striatal high gamma and beta activity may have different functional roles preferentially associated to reinforcement learning and sensorimotor functions, respectively.

The studies mentioned above provide associative evidence linking the presence of reinforcement with changes of neural activity within the striatum determined through neuroimaging[17,18], but do not allow to draw conclusions regarding its causal role in reinforcement motor learning in humans. The only causal evidence available to date comes from animal work showing modulation of reinforcement-based decision-making with striatal stimulation[32,33]. A reason for the current absence of investigations of the causal role of the striatum in human behaviour is related to its deep localization in the brain. As such, current non-invasive brain stimulation techniques, such as transcranial magnetic stimulation (TMS) or classical transcranial electric stimulation (tES), do not allow to selectively target deep brain regions, because these techniques exhibit a steep depth-focality trade-off[34,35]. Studies of patients with lesions of the striatum[36,37] or invasive deep brain stimulation of connected nuclei[38,39] have provided insights into the role of the basal ganglia in reinforcement learning. However, their conclusions are partially limited by the fact that the studied patients also have altered network properties resulting from neurodegeneration, lesions or respective compensatory mechanisms and therefore do not allow to conclude comprehensively regarding the role of the striatum in the physiological state. Here, we address these challenges by exploiting transcranial electric Temporal Interference Stimulation (tTIS), a new non-invasive brain stimulation approach allowing to target deep brain regions in a frequency-specific and focal manner[40,41].

The concept of tTIS was initially proposed and validated on the hippocampus of rodents[40] and was then further tested through computational modelling[42–46] and in first applications on cortical areas in humans[47,48]. tTIS requires two pairs of electrodes to be placed on the head, each pair delivering a high frequency alternating current. One key element is that this frequency has to be high enough (i.e., in the kHz range) to avoid direct neuronal entrainment, based on the low filtering properties of neuronal membranes[49]. The second key element consists in applying a small difference of frequency between the two alternating currents. The superposition of the electric fields creates an envelope oscillating at this low-frequency difference, which can be steered towards individual deep brain structures (e.g., by optimizing electrodes' placement), and is in a range able to influence neuronal activity [40,50–52]. An interesting feature of tTIS is to stimulate at a particular frequency of interest in order to preferentially interact with specific neuronal processes[40,41]. Importantly, despite these exciting opportunities, current evidence for tTIS-related neuromodulation of deep brain structures, such as the striatum, is lacking in humans.

Here, we combine tTIS with electric field modelling for target localisation, behavioural data and functional magnetic resonance imaging (fMRI) to evaluate the causal role of specific striatal oscillations in reinforcement learning of motor skills. In particular, based on the studies mentioned above, we hypothesized that striatal tTIS at high gamma frequency ($tTIS_{80Hz}$) would disturb the fine-tuning of high gamma oscillatory activity in the striatum and thereby would perturb reinforcement motor learning in contrast to beta ($tTIS_{20Hz}$) or sham ($tTIS_{Sham}$) stimulation. In line with our prediction, we report that $tTIS_{80Hz}$ disrupted motor learning compared to the controls, but only in the presence of reinforcement. To evaluate the potential neural correlates of these behavioral effects, we measured BOLD activity in the striatum and effective connectivity between the striatum and frontal cortical areas involved in reinforcement motor learning. We found that the disruptive effect of $tTIS_{80Hz}$ on reinforcement learning was associated to a specific modulation of BOLD activity in the putamen and caudate, but not in the cortex, supporting the ability of tTIS to

selectively modulate striatal activity without affecting overlying cortical areas. Moreover, $tTIS_{80Hz}$ also increased the neuromodulatory influence of the striatum on frontal cortical areas involved in reinforcement motor learning. Overall, the present study shows for the first time that tTIS can non-invasively and selectively modulate a striatal mechanism involved in reinforcement learning and opens new horizons for the study of causal relationships between deep brain structures and human behaviour.

2. Results

24 healthy participants (15 women, 25.3 ± 0.1 years old; mean ± SE) performed a force tracking task in the MRI with concurrent tTIS of the striatum. The task required participants to modulate the force applied on a hand-grip force sensor in order to track a moving target with a cursor with the right, dominant hand[53,54] (**Figure 1A**). At each block, participants had to learn a new pattern of motion of the target (**Figure S1**; see Methods). In $Reinf_{ON}$ blocks, participants were provided with online reinforcement feedback during training, giving them real-time information about success or failure throughout the trial, indicated as a green or red target, respectively (please see **Video S1** for the task). The reinforcement feedback was delivered according to a closed-loop schedule, considering previous performance to update the success criterion for each sample[8]. In $Reinf_{OFF}$ blocks, participants practiced with a visually matched random feedback (cyan/magenta). Importantly, in both types of blocks, training was performed with intermittent visual feedback of the cursor, a condition known to maximise the effect of reinforcement on motor learning[4,55–57]. Before and after training, participants performed Pre- and Post-training assessments with full visual feedback, no reinforcement and no tTIS, allowing us to evaluate motor learning. To assess the effect of tTIS on reinforcement-related benefits in motor learning and the associated neural changes, participants performed 6 blocks of 36 trials in the MRI, with concurrent tTIS during training, delivered with a Δf of 20 Hz ($tTIS_{20Hz}$), 80 Hz ($tTIS_{80Hz}$) or as a sham ($tTIS_{Sham}$; 3 $tTIS_{TYPE}$ x 2 $Reinf_{TYPE}$ conditions; **Figure 1B, 1C**). To determine the best electrode montage to stimulate the human striatum (putamen, caudate and nucleus accumbens [NAc] bilaterally), computational modelling with a realistic head model was conducted with Sim4Life[58] (see Methods). The selected montage (F3-F4; TP7-TP8) generated a theoretical temporal interference electric field that was ~30-40% stronger in the striatum than in the overlying cortex, reaching magnitudes of 0.5 to 0.6 V/m (**Figure 1D, 1E**), which are compatible with the field strengths known to induce neuronal entrainment[59–63].

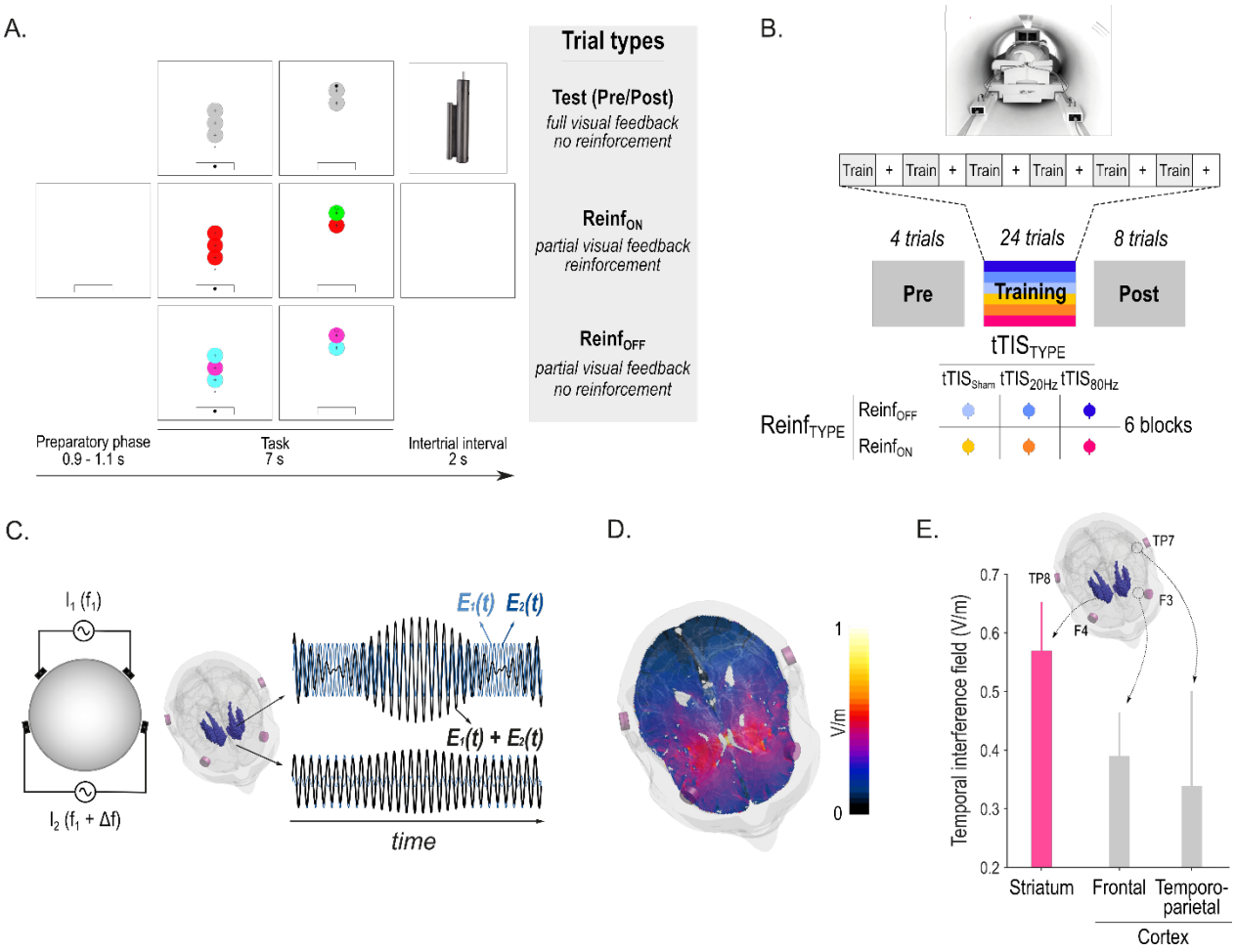

Figure 1. Striatal tTIS during reinforcement learning of motor skills in the MRI. A) Motor learning task. Participants were required to squeeze a hand grip force sensor (depicted in the upper right corner of the figure) in order to track a moving target (larger circle with a cross in the center) with a cursor (black smaller circle)[53,54]. Pre- and Post-training assessments were performed with full visual feedback of the cursor and no reinforcement. In Reinf$_{ON}$ and Reinf$_{OFF}$ trials, participants practiced the task with or without reinforcement feedback, respectively. As such, in Reinf$_{ON}$ trials, the color of the target varied in real-time as a function of the subjects' tracking performance. **B) Experimental procedure.** Participants performed the task in the MRI with concomitant TI stimulation. Blocks of training were composed of 36 trials (4 Pre-, 24 Training and 8 Post-training trials) interspersed with short resting periods (represented as + on the figure). The 6 training types resulted from the combination of 3 tTIS$_{TYPES}$ and 2 Reinf$_{TYPES}$. **C) Concept of tTIS.** On the left, two pairs of electrodes are shown on a head model and currents are applied with a frequency f1 and f1+Δf. On the right, the interference of the two electric fields within the brain is represented for two different locations with respectively high and low envelope modulation. $E_1(t)$ and $E_2(t)$ represent the modulation of the fields' magnitude over time. tTIS was delivered either with a Δf of 20 or 80 Hz or as a sham (ramp-up and immediate ramp-down of high frequency currents with flat envelope). **D) Electric field modelling with the striatal montage.** Temporal interference exposure (electric field modulation magnitude). **E) Temporal interference exposure averaged in the striatum and in the overlying cortex.** Magnitude of the field in the cortex was extracted from the Brainnetome atlas (BNA[64]) regions underneath the stimulation electrodes (F3-

F4 and TP7-TP8). Error bars represent the standard deviation over the voxels in the considered region.

$tTIS_{80Hz}$ disrupts reinforcement learning of motor skills

Performance on the task was evaluated by means of the Error, which was defined as the absolute difference between the applied and target force averaged across samples for each trial, as done previously[4,53,55] (**Figure 2A**). Across conditions, the Post-training Error was reduced compared to the Pre-training Error (single sample t-test on the normalised Post-training data: $t_{(24)}$=-2.69; p=0.013; Cohen's d=-0.55), indicating significant motor learning during the task (**Figure 2B**). Such improvement was greater when participants had trained with reinforcement ($Reinf_{TYPE}$ effect in the Linear Mixed Model (LMM): $F_{(1,\ 1062.2)}$=5.17; p=0.023; d=-0.14 for the post-hoc contrast $Reinf_{ON}$ – $Reinf_{OFF}$), confirming the beneficial effect of reinforcement on motor learning[7,57]. Crucially though, this effect depended on the type of stimulation applied during training ($Reinf_{TYPE}$ x $tTIS_{TYPE}$ interaction: $F_{(2,\ 1063.5)}$=2.11; p=0.034; **Figure 2C**). While reinforcement significantly improved learning when training was performed with $tTIS_{Sham}$ (p=0.036; d=-0.22) and $tTIS_{20Hz}$ (p=0.0089; d=-0.27), this was not the case with $tTIS_{80Hz}$ (p=0.43; d=0.083). Consistently, direct between-condition comparisons showed that in the $Reinf_{ON}$ condition, learning was reduced with $tTIS_{80Hz}$ compared to $tTIS_{20Hz}$ (p=0.039; d=0.26) and $tTIS_{Sham}$ (p<0.001; d=0.45), but was not different between $tTIS_{20Hz}$ and $tTIS_{Sham}$ (p=0.15; d=0.20). This disruption of motor learning with $tTIS_{80Hz}$ was not observed in the absence of reinforcement ($tTIS_{80Hz}$ vs. $tTIS_{20Hz}$: p=0.59; d=-0.10, $tTIS_{80Hz}$ vs. $tTIS_{Sham}$: p=0.34; d=0.15). These results strongly point to the fact that high gamma striatal tTIS specifically disrupts the benefits of reinforcement on motor learning and not motor learning in general.

Although training with $tTIS_{20Hz}$ did not alter the benefits of reinforcement on motor learning, we found that learning without reinforcement was significantly impaired in this condition ($tTIS_{20Hz}$ vs. $tTIS_{Sham}$: p=0.046; d=0.25, **Figure 2C**). This suggests that $tTIS_{20Hz}$ may disrupt a qualitatively

different mechanism involved in learning from sensory feedback[65], in line with the role of striatal beta oscillations in sensorimotor function[28].

As a next step, we evaluated the effect of tTIS on motor performance during training itself. As shown in Figure 2A, the Error was generally higher during Training than in Test trials due to the presence of visual uncertainty during this phase. The extent of this disruption was reduced in the presence of reinforcement ($Reinf_{TYPE}$: $F_{(1,\ 3262.4)}$=339.89; p<0.001; d=-0.64 for the contrast $Reinf_{ON}$ – $Reinf_{OFF}$), demonstrating the ability of subjects to exploit real-time reinforcement information to improve tracking (**Figure 2D**). Notably, this effect was not modulated by $tTIS_{TYPE}$ ($Reinf_{TYPE}$ x $tTIS_{TYPE}$: $F_{(2,\ 3265.8)}$=0.91; p=0.40), indicating that tTIS did not directly influence reinforcement gains during tracking. Interestingly though, striatal stimulation did impact on general tracking performance independently of reinforcement as indicated by a significant $tTIS_{TYPE}$ effect ($tTIS_{TYPE}$: $F_{(2,\ 3262.4)}$=42.85; p<0.001). This effect was due to an increase in the Error when $tTIS_{20Hz}$ was applied (p<0.001; d=0.28 when compared to $tTIS_{Sham}$), which was even stronger during $tTIS_{80Hz}$ (p<0.001; d=0.38 and p=0.031; d=0.11 when compared to $tTIS_{Sham}$ and $tTIS_{20Hz}$, respectively). These results suggest that striatal tTIS altered motor performance in a frequency-dependent manner, but did not influence the ability to rapidly adjust motor commands based on reinforcement feedback during training. Hence, $tTIS_{80Hz}$ may not disrupt real-time processing of reinforcement feedback, but may rather impair the beneficial effect of reinforcements on the retention of motor memories[6,7].

Notably, this effect could not be explained by potential differences in initial performance between conditions ($Reinf_{TYPE}$ x $tTIS_{TYPE}$: $F_{(2,\ 519.99)}$=1.08; p=0.34), nor by changes in the flashing properties of the reinforcement feedback (i.e., the frequency of color change during tracking; $Reinf_{TYPE}$ x $tTIS_{TYPE}$: $F_{(2,\ 3283)}$=0.19; p=0.82), or by differences in success rate in the $Reinf_{ON}$ blocks (i.e., the proportion of success feedback during tracking; $tTIS_{TYPE}$: $F_{(2,\ 1702)}$=0.17; p=0.84; see **Supplementary materials**).

Finally, these results can also not be a consequence of an inefficient blinding. As such, when debriefing after the experiment, only 6/24 participants were able to successfully identify the order of the stimulation applied (e.g., real – real – placebo; chance level: 4/24; Fisher exact test on proportions: p=0.74). Consistently, the magnitude (**Figure S2A**) and type (**Figure S2B**) of tTIS-evoked sensations evaluated before the experiment were qualitatively similar across conditions and tTIS was generally well tolerated in all participants (no adverse events reported). This suggests that blinding was successful and is unlikely to explain our findings. More generally, this is a first indication that tTIS evokes very limited sensations (e.g., only 2/24 and 1/24 subjects rated sensations evoked at 2 mA as "strong" for $tTIS_{20Hz}$ and $tTIS_{80Hz}$, respectively; **Figure S2A**) that are compatible with efficient blinding.

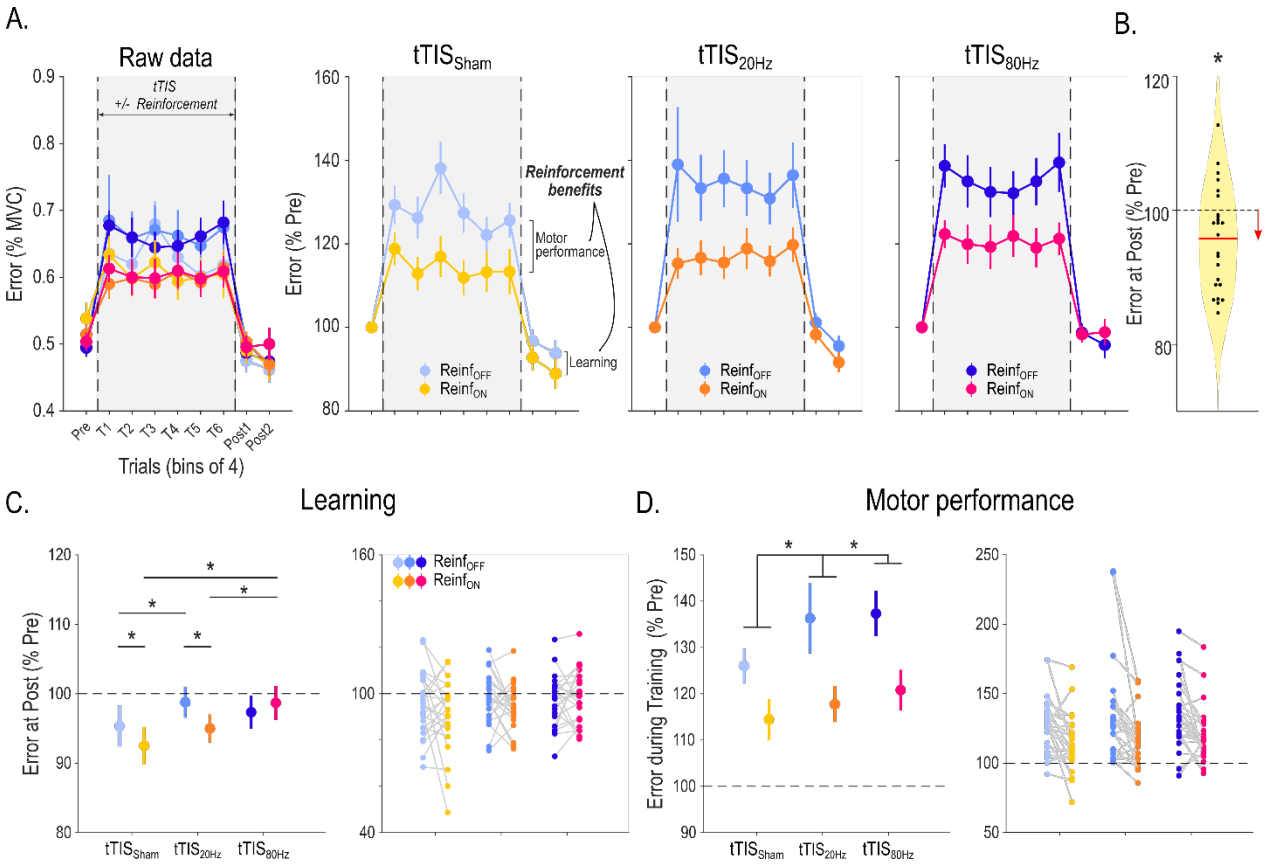

Figure 2. Behavioural results. A) Motor performance across training. Raw Error data (expressed in % of Maximum Voluntary Contraction [MVC]) are presented on the left panel for the different experimental conditions in bins of 4 trials. The increase in Error during Training is related to the visual uncertainty (i.e., intermittent disappearance of the cursor) that was applied to enhance

reinforcement effects. On the right, the three plots represent the Pre-training normalised Error in the $tTIS_{Sham}$, $tTIS_{20Hz}$ and $tTIS_{80Hz}$ blocks. Reinforcement-related benefits represent the improvement in the Error measured in the $Reinf_{ON}$ and $Reinf_{OFF}$ blocks, during Training (reflecting benefits in motor performance) or at Post-training (reflecting benefits in learning). **B) Averaged learning across conditions.** Violin plot showing the Error distribution at Post-training (expressed in % of Pre-training) averaged across conditions, as well as individual subject data. A single-sample t-test showed that the Post-training Error was reduced compared to the Pre-training level, indicating significant learning in the task. **C) Motor learning.** Averaged Error at Post-training (normalised to Pre-training) and the corresponding individual data points in the different experimental conditions are shown on the left and right panels, respectively. Reduction of Error at Post-training reflects true improvement at tracking the target in Test conditions (in the absence of reinforcement, visual uncertainty or tTIS). The LMM ran on these data revealed a specific effect of $tTIS_{80Hz}$ on reinforcement-related benefits in learning. **D) Motor performance.** Averaged Error during Training (normalised to Pre-training) and the corresponding individual data points in the different experimental conditions are shown on the left and right panels, respectively. Individual data points are shown on the right panel. Error change during Training reflect the joint contribution of the experimental manipulations (visual uncertainty, potential reinforcement and tTIS) on motor performance. The LMM ran on these data showed a frequency-dependent effect of tTIS on motor performance, irrespective of reinforcement. *: $p<0.05$. Data are represented as mean ± SE.

The effect of $tTIS_{80Hz}$ on reinforcement motor learning is related to modulation of neural activity in the striatum

As mentioned above, task-based fMRI was acquired during Training with concomitant tTIS. This allowed us to evaluate the neural effects of tTIS and their potential relationship to the behavioural effects reported above. As a first qualitative evaluation of the data, we performed a whole-brain analysis in the $tTIS_{Sham}$ condition to assess the network activated during reinforcement motor learning ($Reinf_{ON}$ condition). Consistent with previous neuroimaging studies employing similar tasks[66,67], we found prominent BOLD activations in a motor network including the putamen, thalamus, cerebellum and sensorimotor cortex, particularly on the left hemisphere, contralateral to the trained hand (**Figure S3, Table S2**). Notably though, contrasting $Reinf_{ON}$ and $Reinf_{OFF}$ conditions did not reveal any significant cluster at the whole-brain level.

As a second step, we evaluated the effect of tTIS on striatal activity, as a function of the type of reinforcement feedback and focusing on the very same regions of interest (ROI) that were used to optimise tTIS exposure in the modelling. Based on this, we extracted averaged BOLD

activity within the bilateral putamen, caudate and NAc based on the Brainnetome atlas (BNA[64]), in the different experimental conditions and considered these six striatal ROIs (ROI_{STR}) as fixed effects in the LMM. This model revealed a strong enhancement of striatal activity with $Reinf_{ON}$ with respect to $Reinf_{OFF}$ ($F_{(1,\ 800.01)}$=13.23; p<0.001; d=0.25 for the contrast $Reinf_{ON}$ – $Reinf_{OFF}$) consistent with previous literature[11], but no $tTIS_{TYPE}$ effect ($F_{(2,\ 800.01)}$=0.46; p=0.63) and no interaction effect (all p> 0.65; **Figure 3A**). Despite the absence of effects of tTIS on averaged striatal activity, we then asked whether the behavioural effects of $tTIS_{80Hz}$ on reinforcement motor learning (i.e., $tTIS_{80Hz}$ vs. $tTIS_{20Hz}$ and $tTIS_{Sham}$ with $Reinf_{ON}$) could be linked to modulation of activity in core brain regions. To do so, we ran a whole-brain analysis focusing on the main behavioural effects mentioned above. Results revealed that the effect of $tTIS_{80Hz}$ (with respect to $tTIS_{20Hz}$) on motor learning in the $Reinf_{ON}$ condition was specifically related to modulation of activity in two clusters encompassing the left putamen and bilateral caudate (**Figure 3B, Table S3**). No significant clusters were found for the $tTIS_{80Hz}$ – $tTIS_{Sham}$ contrast, neither for the control $tTIS_{20Hz}$ - $tTIS_{Sham}$ contrast. Overall, these results provide evidence that the detrimental effect of $tTIS_{80Hz}$ on reinforcement learning of motor skills is related to a specific modulation of oscillatory activity in the striatum, supporting the idea that high gamma striatal oscillations are causally involved in reinforcement learning.

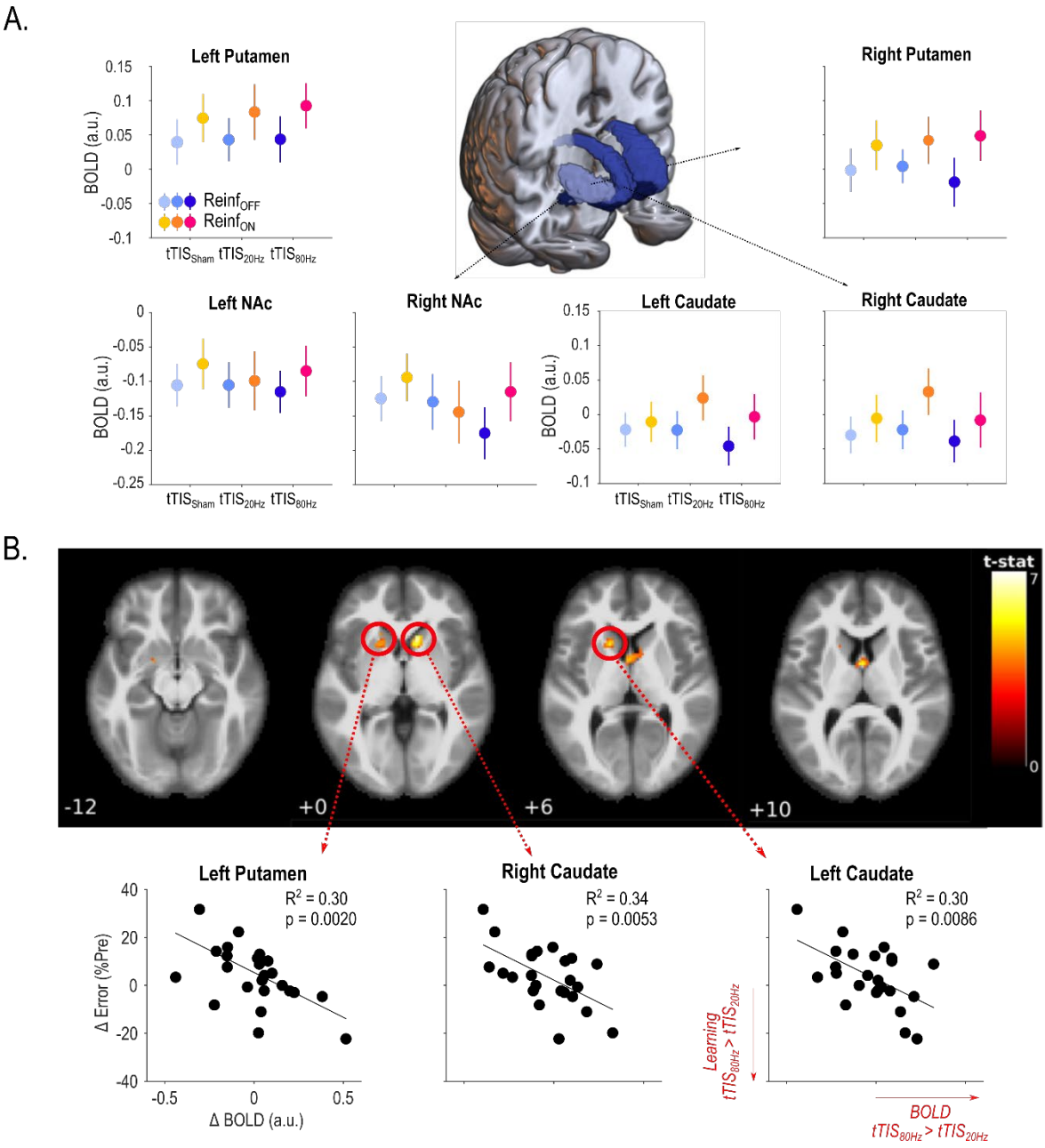

Figure 3. Striatal activity. A) Striatal BOLD responses. A 3D-reconstruction of the striatal masks used in the current experiment is surrounded by plots showing averaged BOLD activity for each mask in the different experimental conditions. A LMM ran on these data showed higher striatal responses in the $Reinf_{ON}$ with respect to the $Reinf_{OFF}$ condition, but no effect of $tTIS_{TYPE}$ and no interaction. **B) Whole-brain activity associated to the behavioural effect of $tTIS_{80Hz}$ on reinforcement motor learning.** Correlation between tTIS-related modulation of striatal activity ($tTIS_{80Hz}$ – $tTIS_{20Hz}$) and learning abilities in the $Reinf_{ON}$ condition. Significant clusters of correlation were found in the left putamen and bilateral caudate (uncorrected voxel-wise FWE: p=0.001, and corrected cluster-based FDR: p=0.05). Lower panel shows individual correlations for the three significant regions highlighted in the whole-brain analysis. *: p<0.05. Data are represented as mean ± SE.

$tTIS_{80Hz}$ enhances effective connectivity between the striatum and frontal cortex.

Interactions between the striatum and frontal cortex are crucial for a variety of behaviours including motor and reinforcement learning[13]. In particular, reinforcement motor learning requires to use information about task success to guide future motor commands[4], a process for which the striatum may play an integrative role at the interface between fronto-striatal loops involved in reward processing and motor control[13,68]. In a subsequent analysis, we asked whether striatal tTIS modulates striatum to frontal cortex communication during reinforcement motor learning. More specifically, we computed effective connectivity (using the generalized psychophysiological interactions method[69]) between striatal and frontal regions classically associated with motor and reward-related functions, and thought to be involved in reinforcement motor learning[70,71]. For the motor network, we evaluated effective connectivity between motor parts of the striatum (i.e., dorso-lateral putamen (dlPu) and dorsal caudate (dCa)) and two regions strongly implicated in motor learning: the medial part of the supplementary motor area (SMA) and the part of the primary motor cortex (M1) associated to upper limb functions (**Figure 4A**). For the reward network, we assessed connectivity between parts of the striatum classically associated to limbic functions (i.e., the NAc and the ventro-medial putamen (vmPu) and two frontal areas involved in reward processing: the anterior cingulate cortex (ACC) and the ventro-medial prefrontal cortex (vmPFC; **Figure 4B;** Bartra et al., 2013). The LMM ran with the fixed effects $Reinf_{TYPE}$, $tTIS_{TYPE}$ and $Network_{TYPE}$ showed a significant effect of $tTIS_{TYPE}$ ($F_{(2, 2264.0)}$=5.42; p=0.0045), that was due to higher connectivity in the $tTIS_{80Hz}$ condition with respect to $tTIS_{Sham}$ (p=0.0038; d=0.16) and $tTIS_{20Hz}$ (at the trend level, p=0.069; d=0.11). There was no difference in connectivity between $tTIS_{20Hz}$ and $tTIS_{Sham}$ (p=0.58; d=0.051). Hence, $tTIS_{80Hz}$, but not $tTIS_{20Hz}$, enhanced effective connectivity between the striatum and frontal cortex during motor training.

The LMM did not reveal any effect of $Reinf_{TYPE}$ ($F_{(1, 2264.0)}$=0.010; p=0.92), $Network_{TYPE}$ ($F_{(1, 2264.0)}$=3.16; p=0.076) and no double interaction (note the trend for a $Reinf_{TYPE}$ x $Network_{TYPE}$ effect

though: $F_{(1, 2264.0)}$=3.52; p=0.061). Yet, we did find a significant $Reinf_{TYPE}$ x $tTIS_{TYPE}$ x $Network_{TYPE}$ interaction ($F_{(2, 2264.0)}$=4.87; p=0.0078). Such triple interaction was related to the fact that $tTIS_{80Hz}$ increased connectivity in the $Reinf_{ON}$ condition in the motor network ($Reinf_{ON}$ vs. $Reinf_{OFF}$: p=0.0012; d=0.33; Figure 4A), while it tended to have the opposite effect in the reward network (p=0.063; d=-0.19; Figure 4B). This increase was not present in any of the two networks when either $tTIS_{Sham}$ or $tTIS_{20Hz}$ were applied (all p> 0.40). Moreover, in the motor network, connectivity in the $Reinf_{ON}$ condition was higher with $tTIS_{80Hz}$ than with $tTIS_{Sham}$ (p<0.001; d=0.42) and $tTIS_{20Hz}$ (at the trend level; p=0.059; d=0.23, Figure 4A). These data suggest that $tTIS_{80Hz}$ enhanced the neuromodulatory influence of the striatum on motor cortex during task performance, but only in the presence of reinforcement. In the reward network, post-hocs revealed that connectivity in the $Reinf_{OFF}$ condition was significantly higher with $tTIS_{80Hz}$ compared to $tTIS_{20Hz}$ (p=0.045; d=0.25; Figure 4B), in line with the general effect of $tTIS_{TYPE}$ on connectivity reported above. This pattern of results suggests that the increase of connectivity from striatum to frontal cortex observed with $tTIS_{80Hz}$ depends on the presence of reinforcement, in particular in the motor network. Such reinforcement-dependent increase of connectivity may reflect the preferential entrainment of striatal gamma oscillations with $tTIS_{80Hz}$[59] in a situation where these oscillations are already boosted by the presence of reinforcement[19] (see Discussion).

Notably, contrary to the BOLD results presented above, we did not find any correlations between the effects of $tTIS_{80Hz}$ on connectivity and motor learning, neither in the motor (robust linear regression: $tTIS_{80Hz}$ – $tTIS_{Sham}$: R^2=0.019; p=0.48; $tTIS_{80Hz}$ – $tTIS_{20Hz}$: R^2=0.034; p=0.54) nor in the reward ($tTIS_{80Hz}$ – $tTIS_{Sham}$: R^2=0.037; p=0.46; $tTIS_{80Hz}$ – $tTIS_{20Hz}$: R^2<0.001; p=0.75) network, suggesting some degree of independence between the effect of $tTIS_{80Hz}$ on reinforcement motor learning and on effective connectivity.

As a control, we verified that the effects of $tTIS_{TYPE}$ on connectivity could not be observed in a control network associated to language (as defined by [72]), which was unlikely to be involved

in the present task and did not include the striatum (see Methods). As expected, effective connectivity within the language network was not modulated by $Reinf_{TYPE}$ ($F_{(1, 547)}$=0.81; p=0.37), nor by $tTIS_{TYPE}$ ($F_{(2, 547)}$=0.58; p=0.56), or by $Reinf_{TYPE}$ x $tTIS_{TYPE}$ ($F_{(2, 547)}$=0.45; p=0.64).

Overall, these results highlight the ability of $tTIS_{80Hz}$, but not $tTIS_{20Hz}$, to modulate striatum to frontal cortex connectivity. Moreover, they suggest that a potential mechanism of action of $tTIS_{80Hz}$ is the induction of a state of hyper-connectivity between striatum and motor cortex that may be detrimental for reinforcement motor learning.

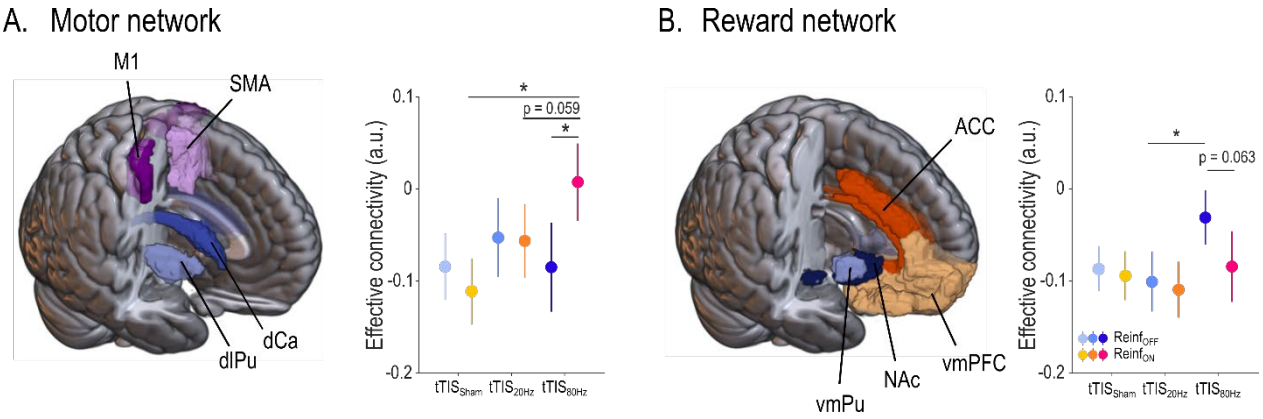

Figure 4. Striatum to frontal cortex effective connectivity. A) Motor network. On the left, 3D reconstruction of the masks used for the motor network (i.e., dorso-lateral putamen, dorsal caudate, M1, SMA). On the right, plot showing effective connectivity from motor striatum to motor cortex in the different experimental conditions. Note the increase of connectivity with $tTIS_{80Hz}$ in the presence of reinforcement. **B) Reward network.** On the left, 3D reconstruction of the masks used for the reward network (i.e., ventro-medial putamen, NAc, vmPFC, ACC). On the right, plot showing effective connectivity from motor striatum to motor cortex in the different experimental conditions. ROIs were defined based on the BNA atlas[12] *: p<0.05. Data are represented as mean ± SE.

Neural effects of $tTIS_{80Hz}$ depend on impulsivity

Determining individual factors that shape responsiveness to non-invasive brain stimulation approaches is a crucial step to better understand the mechanisms of action but also to envision stratification of patients in future clinical interventions[73]. A potential factor that could explain inter-individual differences in responsiveness to $tTIS_{80Hz}$ is the level of impulsivity. As such, impulsivity has been associated to changes of gamma oscillatory activity in the striatum of rats[74] and to the activity of fast-spiking interneurons in the striatum[75,76], a neuronal population that is strongly entrained to gamma rythms[19,21] and may therefore be particularly sensitive to $tTIS_{80Hz}$. In a subsequent exploratory analysis, we asked if the neural effects of $tTIS_{80Hz}$ were associated to impulsivity levels, as evaluated by a well-established independent delay-discounting questionnaire performed at the beginning of the experiment[77,78]. Strikingly, a whole-brain analysis revealed that impulsivity was associated to the effect of $tTIS_{80Hz}$ on BOLD activity (with respect to $tTIS_{20Hz}$) specifically in the left caudate nucleus (**Figure S4A, S4B, Table S4**). Moreover, the effect of $tTIS_{80Hz}$ on striatum to motor cortex connectivity reported above was negatively correlated to impulsivity both when contrasting $tTIS_{80Hz}$ with $tTIS_{Sham}$ (**Figure S4C, left**) and with $tTIS_{20Hz}$ (**Figure S4C, middle**). Such correlations were absent when contrasting $tTIS_{20Hz}$ with $tTIS_{Sham}$ (**Figure S4C, right**), as well as when considering the same contrasts in the reward instead of the motor network (see Supplementary materials for more details). Taken together, these results suggest that inter-individual variability in impulsivity might influence the neural responses to striatal $tTIS_{80Hz}$.

3. Discussion

In this study, we combined striatal tTIS with electric field modelling, behavioural and fMRI analyses to evaluate the causal role of the striatum in reinforcement learning of motor skills in healthy humans. $tTIS_{80Hz}$, but not $tTIS_{20Hz}$, disrupted the ability to learn from reinforcement feedback. This behavioural effect was associated to modulation of neural activity specifically in the striatum. As a second step, we show that $tTIS_{80Hz}$, but not $tTIS_{20Hz}$, increased the neuromodulatory influence of the striatum on connected frontal cortical areas involved in reinforcement motor learning. Finally, inter-individual variability in the neural effects of $tTIS_{80Hz}$ could be partially explained by impulsivity, suggesting that this trait may constitute a determinant of responsiveness to high gamma striatal tTIS. Overall, the present study shows for the first time that striatal tTIS can non-invasively modulate a striatal mechanism involved in reinforcement learning, opening new horizons for the study of causal relationships between deep brain structures and human behaviour.

In this work, we investigated the causal role of the human striatum in reinforcement learning of motor skills in healthy humans; a question that cannot be addressed with conventional non-invasive brain stimulation techniques. In particular, by stimulating at different frequencies, we aimed at dissociating striatal mechanisms involved in reinforcement and sensorimotor learning. In line with our main hypothesis, we found that striatal $tTIS_{80Hz}$ altered reinforcement learning of a motor skill. Such disruption was frequency- and reinforcement-specific: learning was not altered with striatal $tTIS_{20Hz}$ in the presence of reinforcement, or when striatal $tTIS_{80Hz}$ was delivered in the absence of reinforcement. The rationale to stimulate at high gamma frequency was based on previous work showing reinforcement-related modulation of gamma oscillations in the striatum[19–21,24,26,74,79] and in the frontal cortex[79–82]. Several neuronal mechanisms may contribute to the

detrimental effect of $tTIS_{80Hz}$ on reinforcement motor learning. First, as it consisted in a constant high gamma oscillating field applied on the striatum, $tTIS_{80Hz}$ may have perturbed the fine-tuned reinforcement-dependent modulation of high gamma oscillatory activity[19–21,25–27], preventing participants to learn from different outcomes. Another potential explanation is that $tTIS_{80Hz}$ disrupted the temporal coordination of striatal gamma activity to interacting ongoing rhythmic activity, a mechanism that has been previously associated to reinforcement learning in humans[25]. Finally, the applied stimulation was not personalized as it did not take into account the individual high gamma frequency peak associated to reward processing and the potential heterogeneity of gamma activity within the striatum[24]. Hence, $tTIS_{80Hz}$ may have resulted in a frequency mismatch between the endogenous high gamma activity and the externally imposed rhythm, that could paradoxically result in a reduction of neuronal entrainment, in particular when the frequency mismatch is relatively low[60]. Importantly, in contrast to striatal $tTIS_{80Hz}$, we found that $tTIS_{20Hz}$ reduced learning, but only in the absence of reinforcement. This result fits well with the literature linking striatal beta oscillations to sensorimotor functions[28,29,31,83–85]. Taken together, these elements suggest that different oscillations within the striatum support qualitatively distinct motor learning mechanisms with beta activity contributing mostly to sensory-based learning and high gamma activity being particularly important for reinforcement learning. More generally, these results add to the growing body of evidence showing that sensory- and reinforcement-based motor learning rely on partially different neural mechanisms[8,9,65,71,86,87].

Interestingly, striatal tTIS (especially $tTIS_{80Hz}$) also impaired tracking performance during training, irrespective of the presence of reinforcement. This frequency-dependent reduction of motor performance may be due to altered neuronal processing in the sensorimotor striatum that may lead to less fine-tuned motor control abilities[88]. Importantly though, tTIS did not modulate the ability of participants to benefit from real-time reinforcement feedback during motor performance.

443 This suggests that striatal $tTIS_{80Hz}$ altered the beneficial effects of reinforcement on learning (as
444 evaluated in Test conditions at Post-training), but not on motor performance (as evaluated during
445 Training). Such dissociation between the effects of striatal $tTIS_{80Hz}$ on reinforcement-related gains
446 in motor performance and learning may be explained by the fact that these two phases of the
447 protocol probe different processes[55,89]. While improvement of motor performance with
448 reinforcement feedback relies on rapid adjustments of motor output based on recent outcomes[90],
449 reinforcement gains in learning (i.e., probed in Test conditions without reinforcement) may rather
450 reflect the beneficial effect of performance feedback on the retention of motor memories[7,53].
451 Hence, a potential explanation for the present results is that striatal $tTIS_{80Hz}$ did not disrupt real-
452 time processing of reinforcement feedback, but may rather alter the strengthening of the memory
453 trace based on reinforcements[6,7]. Overall, these results are consistent with the view that specific
454 patterns of oscillatory activity in the striatum are causally involved in motor control and learning
455 processes[31], and can be modulated with electrical stimulation[59,61,91].

456

457 To better understand the neural effects and frequency-specificity of tTIS, we coupled
458 striatal tTIS and task performance with simultaneous fMRI acquisition. The imaging results support
459 the view that the effect of $tTIS_{80Hz}$ on reinforcement learning of motor skills was indeed related to
460 neuromodulation of the striatum. As such, when considering averaged BOLD activity, we found a
461 general increase of striatal activity when reinforcement was provided[11], but no effect of tTIS.
462 Crucially though, the detrimental effect of $tTIS_{80Hz}$ on reinforcement learning was related to a
463 specific modulation of activity in the caudate and putamen, providing evidence that the present
464 behavioural effects were indeed driven by focal neuromodulation of the striatum (Figure 3).
465 Interestingly, participants with stronger disruption of reinforcement learning at the behavioural
466 level were also the ones exhibiting stronger suppression of striatal activity with $tTIS_{80Hz}$ (compared
467 to $tTIS_{20Hz}$), suggesting that tTIS-induced reduction of striatal activity is detrimental for
468 reinforcement motor learning. Further analyses showed that $tTIS_{80Hz}$, but not $tTIS_{20Hz}$, increased

the neuromodulatory influence of the striatum on frontal areas known to be important for motor learning and reinforcement processing[92,93]. Interestingly, this effect depended on the type of network considered (reward vs. motor) and on the presence of reinforcement. Striatal $tTIS_{80Hz}$ coupled with reinforcement increased connectivity between the motor striatum and the motor cortex while it tended to have the opposite effect when considering the connectivity between limbic parts of the striatum and pre-frontal areas involved in reward processing (Figure 4). This result may reflect the differential influence of striatal tTIS on distinct subparts of the striatum, depending on their pattern of activity during the task[51]. As such, a recent study in non-human primates showed that tACS can have opposite effects on neuronal activity based on the initial entrainment of neurons to the target frequency[60]. Hence, the present differential effects of $tTIS_{80Hz}$ on motor and reward striato-frontal pathways may be due to different initial patterns of activity in these networks in the presence of reinforcement. Electrophysiological recordings with higher temporal resolution than fMRI are required to confirm or infirm this hypothesis. Overall, the present neuroimaging results support the idea that the behavioural effects of striatal $tTIS_{80Hz}$ on reinforcement learning are associated to a selective modulation of striatal activity that influence striato-frontal communication.

Finding individual factors that influence responsiveness to brain stimulation is an important line of research both for fundamental neuroscience but also to characterise profiles of responders for future clinical translation[73]. Based on previous literature linking striatal gamma oscillatory mechanisms and impulsivity, we explored the possibility that impulsivity influences responsiveness to striatal $tTIS_{80Hz}$ (Figure S4). Consistent with this idea, we found that impulsivity was associated to $tTIS_{80Hz}$-related BOLD changes specifically in the left caudate and to changes of effective connectivity between the motor striatum and motor cortex during reinforcement motor learning. Hence, a possibility is that the differences in endogenous striatal gamma-related activity

494 that have been associated to impulsive behaviour in animal models[74–76], influence the neural
495 effects of $tTIS_{80Hz}$. If this is the case, impulsivity could constitute a behavioural factor allowing to
496 determine responsiveness to striatal $tTIS_{80Hz}$. Conversely, an interesting avenue for future
497 research could aim at determining whether impulsivity can be modulated by striatal $tTIS_{80Hz}$.

498

499 From a methodological point of view, the present results provide new experimental support
500 to the idea that the effects of tTIS are related to amplitude modulation of electric fields deep in the
501 brain and not to the high frequency fields themselves, in line with recent work[40,41,51]. As such, the
502 different behavioural and neural effects of striatal $tTIS_{80Hz}$ and $tTIS_{20Hz}$ despite comparable carrier
503 frequencies (centered on 2kHz) indicate that temporal interference was indeed the driving force
504 of the present effects. Moreover, disruption of reinforcement motor learning with $tTIS_{80Hz}$ (relative
505 to $tTIS_{20Hz}$) was specifically related to neuromodulation of the striatum, where the amplitude of the
506 tTIS field was highest according to our simulations (see [52,94] for recent validations of comparable
507 simulations in cadavers experiments). Hence, we believe that the frequency- and reinforcement-
508 dependent tTIS effects reported here cannot be explained by direct modulation of neural activity
509 by the high frequency fields. Yet, disentangling the neural effects of the low-frequency envelope
510 and the high frequency carrier appears as an important next step to better characterise the
511 mechanisms underlying tTIS[46].

512

513 **Conclusion**

514 The present findings show for the first time the ability of non-invasive striatal tTIS to
515 interfere with reinforcement learning in humans through a selective modulation of striatal activity.
516 Such deep brain stimulation was well tolerated and compatible with efficient blinding, suggesting
517 that tTIS provides the exciting option to circumvent the steep depth-focality trade-off of current

518 non-invasive brain stimulation approaches in a safe and effective way. Overall, tTIS opens new
519 possibilities for the study of causal brain-behaviour relationships and for the treatment of neuro-
520 psychiatric disorders associated to alterations of deep brain structures.

4. Methods

4.1. Participants

A total of 24 right-handed healthy volunteers participated in the present study (15 women, 25.3 ± 0.1 years old; mean ± SE). Handedness was determined via a shortened version of the Edinburgh Handedness inventory[95] (laterality index = 89.3 ± 2.14%). None of the participants suffered from any neurological or psychiatric disorder, nor taking any centrally-acting medication (see Supplementary Materials for a complete list of exclusion criteria). All participants gave their written informed consent in accordance with the Declaration of Helsinki and the Cantonal Ethics Committee Vaud, Switzerland (project number 2020-00127). Finally, all participants were asked to fill out a delay-discounting monetary choice questionnaire[96], which evaluates the propensity of subjects to choose smaller sooner rewards over larger later rewards, a preference commonly associated to choice impulsivity[77,97].

4.2. Experimental procedures

The study employed a randomised, double-blind, sham-controlled design. Following screening and inclusion, participants were invited to a single experimental session including performance of a motor learning task with concurrent transcranial electric Temporal Interference stimulation (tTIS) of the striatum and functional magnetic resonance imaging (fMRI). Overall, participants practiced 6 blocks of trials, that resulted from the combination of two reinforcement feedback conditions ($Reinf_{TYPE}$: $Reinf_{ON}$ or $Reinf_{OFF}$) with three types of striatal stimulation ($tTIS_{TYPE}$: $tTIS_{Sham}$, $tTIS_{20Hz}$ or $tTIS_{80Hz}$).

4.2.1. Motor learning task

4.2.1.1. General aspects

Participants practiced an adaptation of a widely used force-tracking motor task (Abe et al., 2011, Steel et al., 2016) with a fMRI-compatible fiber optic grip force sensor (Current designs, Inc., Philadelphia, PA, USA) positioned in their right hand. The task was developed on Matlab 2018 (the Mathworks, Natick, Massachusetts, USA) exploiting the Psychophysics Toolbox extensions[98,99] and was displayed on a computer screen with a refresh rate of 60 Hz. The task required participants to squeeze the force sensor to control a cursor displayed on the screen. Increasing the exerted force resulted in the cursor moving vertically and upward in a linear way. Each trial started with a preparatory period in which a sidebar appeared at the bottom of the screen (**Figure 1A**). After a variable time interval (0.9 to 1.1 s), a cursor (black circle) popped up in the sidebar and simultaneously a target (grey larger circle with a cross in the middle) appeared, indicating the start of the movement period. Subjects were asked to modulate the force applied on the transducer to keep the cursor as close as possible to the center of the target. The target moved in a sequential way along a single vertical axis for 7 s. The maximum force required (i.e., the force required to reach the target when it was in the uppermost part of the screen; $MaxTarget_{Force}$) was set at 4% of maximum voluntary contraction (MVC) evaluated at the beginning of the experiment. This low force level was chosen based on pilot experiments to limit muscular fatigue. Finally, each trial ended with a blank screen displayed for 2 s before the beginning of the next trial.

4.2.1.2. Trial types and reinforcement manipulation

During the experiment, participants were exposed to different types of trials (**Figure 1A, Video S1**). In Test trials, the cursor remained on the screen and the target was consistently

displayed in grey for the whole duration of the trial. These trials served to evaluate Pre- and Post-training performance for each block. In $Reinf_{ON}$ and $Reinf_{OFF}$ trials (used during Training only), we provided only limited visual feedback to the participants in order to increase the impact of reinforcement on learning[4,55–57]. As such, the cursor was only intermittently displayed during the trial: it was always displayed in the first second of the trial, and then disappeared for a total of 4.5 s randomly split on the remaining time by bits of 0.5 s. The cursor was therefore displayed 35.7% of the time during these trials (2.5 s over the 7 s trial). Importantly, contrary to the cursor, the target always remained on the screen for the whole trial and participants were instructed to continue to track the target even when the cursor was away.

In addition to this visual manipulation, in $Reinf_{ON}$ trials, participants also trained with reinforcement feedback indicating success or failure of the tracking in real time. As such, participants were informed that, during these trials, the color of the target would vary as a function of their performance: the target was displayed in green when tracking was considered as successful and in red when it was considered as failure. Online success on the task was determined based on the Error, defined as the absolute force difference between the force required to be in the center of the target and the exerted force[4,53–55]. The Error, expressed in percentage of MVC, was computed for each frame refresh and allowed to classify a sample as successful or not based on a closed-loop reinforcement schedule[8]. More specifically, for each training trial, a force sample was considered as successful if the Error was below the median Error over the 4 previous trials at this specific sample. Put differently, to be successful, participants had to constantly beat their previous performance. This closed-loop reinforcement schedule allowed us to deliver consistent reinforcement feedback across individuals and conditions, while maximizing uncertainty on the presence of reinforcement, an aspect that is crucial for efficient reinforcement motor learning[100]. Notably, in addition to this closed-loop design, samples were also considered as successful if the cursor was very close to the center of the target (i.e., within one

radius around the center, corresponding to an Error below 0.2% of MVC). This was done to prevent any conflict between visual information (provided by the position of the cursor relative to the target) and reinforcement feedback (provided by the color of the target), which could occur in situations of extremely good performance (when the closed-loop Error cut-off is below 0.2% of MVC).

As a control, $Reinf_{OFF}$ trials were similar to $Reinf_{ON}$ trials with the only difference that the displayed colors were either cyan or magenta, and were generated randomly. Participants were explicitly told that, in this condition, colors were displayed randomly and could be ignored. The visual properties of the target in the $Reinf_{OFF}$ condition were designed to match the $Reinf_{ON}$ condition in terms of relative luminance (cyan: RGB = [127.5 242.1 255] matched to green: [127.5 255 127.5] and magenta: [211.7 127.5 255] to red: [255 127.5 127.5]) and average frequency of change in colors (i.e., the average number of changes in colors divided by the total duration of a trial, see Supplementary materials).

4.2.1.3. Motor learning protocol

After receiving standardised instructions about the force-tracking task, participants practiced 5 blocks of familiarization (total of 75 trials) without tTIS. The first block of familiarization included 20 trials with the target moving in a regular fashion (0.5 Hz sinuoid). Then, in a second block of familiarization, participants performed 35 trials of practice with an irregular pattern, with the same properties as the training patterns (see below). Finally, we introduced the reinforcement manipulation and let participants perform 2 short blocks (8 trials each) including $Reinf_{ON}$ and $Reinf_{OFF}$ trials. These four first blocks of familiarization were performed outside the MRI environment. A last familiarization block (4 trials) was performed after installation in the scanner, to allow participants to get used to performing the task in the MRI. This long familiarization allowed

participants to get acquainted with the use of the force sensor, before the beginning of the experiment.

During the main part of the experiment, participants performed 6 blocks of trials in the MRI with concurrent striatal tTIS (**Figure 1B**). Each block was composed of 4 Pre-training trials followed by 24 Training and 8 Post-training trials. Pre- and Post-training trials were performed in Test conditions, without tTIS and were used to evaluate motor learning. Training trials were performed with or without reinforcement feedback and with concomitant striatal tTIS and were used as a proxy of motor performance. During Training, trials were interspersed with 25 s resting periods every 4 trials (used for fMRI contrasts, see below). The order of the 6 experimental conditions was pseudo-randomised across participants: the 6 blocks were divided into 3 pairs of blocks with the same tTIS condition and each pair was then composed of one $Reinf_{ON}$ and one $Reinf_{OFF}$ block. Within this structure, the order of the $tTIS_{TYPE}$ and $Reinf_{TYPE}$ conditions were balanced among the 24 participants.

As mentioned above, the protocol involved multiple evaluations of motor learning within the same experimental session. In order to limit carry-over effects from one block to the following, each experimental block was associated to a different pattern of movement of the target (**Figure S1**). Put differently, in each block, participants had to generate a new pattern of force to successfully track the target. To balance the patterns' difficulty, they all consisted in the summation of 5 sinusoids of variable frequency (range: 0.1-1.5 Hz) that presented the following properties: a) Average force comprised between 45 and 55% of the $MaxTarget_{Force}$; b) Absolute average derivative comprised between 54 and 66 % of the $MaxTarget_{Force}$/s; c) Number of peaks = 14 (defined as an absolute change of force of at least 1% of $MaxTarget_{Force}$). These parameters were determined based on pilot experiments to obtain a relevant level of difficulty for young healthy adults and consistent learning across the different patterns.

4.2.2. Transcranial Electric Temporal Interference Stimulation (tTIS) applied to the striatum

4.2.2.1. General concept

Transcranial temporal interference stimulation (tTIS) is an innovative non-invasive brain stimulation approach, in which two or more independent stimulation channels deliver high-frequency currents in the kHz range (oscillating at f1 and f1 + Δf; **Figure 1C**). These high-frequency currents are assumed to be too high to effectively modulate neuronal activity [40,49,101]. Still, by applying a small shift in frequency, they result in a modulated electric field with the envelope oscillating at the low-frequency Δf (target frequency) where the two currents overlap. The peak of the modulated envelope amplitude can be steered towards specific areas located deep in the brain, by tuning the position of the electrodes and current ratio across stimulation channels[40] (**Figure 1C, 1D**). Based on these properties, tTIS has been shown to be able to focally target activity of deep structures in rodents, without engaging overlying tissues[40]. Here, we applied temporal interference stimulation transcranially via surface electrodes applying a low-intensity, sub-threshold protocol following the currently accepted cut-offs and safety guidelines for low-intensity transcranial electric stimulation in humans[102].

4.2.2.2. Stimulators

The currents for tTIS were delivered by two independent DS5 isolated bipolar constant current stimulators *(Digitimer Ltd, Welwyn Garden City, UK)*. The stimulation patterns were generated using a custom-based Matlab graphical user interface and transmitted to the current sources using a standard digital-analog converter *(DAQ USB-6216, National Instruments, Austin,*

671 *TX, USA)*. Finally, an audio transformer was added between stimulators and subjects, in order to
672 avoid possible direct current accumulation.

673

674 4.2.2.3. Stimulation protocols
675

676 During the 6 Training blocks, we applied three different types of striatal tTIS (2 blocks
677 each): a stimulation with a tTIS envelope modulated at 20Hz ($tTIS_{20Hz}$), a stimulation with a tTIS
678 envelope modulated at 80Hz ($tTIS_{80Hz}$) and a sham stimulation ($tTIS_{Sham}$). For $tTIS_{20Hz}$, the
679 posterior stimulation channel (TP7-TP8, see below) delivered a 1.99 kHz stimulation while the
680 anterior one delivered a 2.01 kHz (Δf = 20 Hz). For $tTIS_{80Hz}$, the posterior and anterior channels
681 delivered 1.96 kHz and 2.04 kHz, respectively (Δf = 80 Hz). Hence in both conditions, the high
682 frequency component was comparable and the only difference was Δf. During each block, tTIS
683 was applied for 5 minutes (6 x 50 s) during Training. Each stimulation period started and ended
684 with currents ramping-up and -down, respectively, for 5 s. tTIS was applied only while participants
685 were performing the motor task and not during resting periods or Pre- and Post-training
686 assessments. Finally, $tTIS_{Sham}$ consisted in a ramping-up (5 s) immediately followed by a ramping-
687 down (5 s) of 2 kHz currents delivered without any shift in frequency. This condition allowed us to
688 mimic the sensations experienced during the active conditions $tTIS_{20Hz}$ and $tTIS_{80Hz}$, while
689 delivering minimal brain stimulation (Figure S2). A trigger was sent 5 seconds before the beginning
690 of each trial in order to align the beginning of the task and the beginning of the frequency shift
691 after the ramp-up. Other TI stimulation parameters were set as follows: current intensity per
692 stimulation channel = 2 mA, electrode type: round, conductive rubber with conductive
693 cream/paste, electrode size = 3 cm^2 (see ContES checklist in Supplementary materials for more
694 details).

695 The stimulation was applied within the MRI environment (Siemens 3T MAGNETOM
696 Prisma; Siemens Healthcare, Erlangen, Germany) using a standard RF filter module and MRI-
697 compatible cables *(neuroConn GmbH, Ilmenau, Germany)*. The technological, safety and noise
698 tests, and methodological factors can be found in Supplementary materials (Table S1) and are
699 based on the ContES Checklist [103].

700

701 4.2.2.4. Modelling

702

703 Electromagnetic simulations were carried out to identify optimised electrode placement
704 and current steering parameters. Simulations were performed using the MIDA head model[58], a
705 detailed anatomical head model featuring >100 distinguished tissues and regions that was derived
706 from multi-modal image data of a healthy female volunteer. Importantly, for brain stimulation
707 modelling, the model differentiates different scalp layers, skull layers, grey and white matter,
708 cerebrospinal fluid, and the dura. Circular electrodes (radius = 0.7 cm) were positioned on the skin
709 according to the 10-10 system and the electromagnetic exposure was computed using the ohmic-
710 current-dominated electro-quasistatic solver from Sim4Life v5.0 (ZMT Zurich MedTech AG,
711 Switzerland), which is suitable due to the dominance of ohmic currents over displacement currents
712 and the long wavelength compared with the simulation domain[104]. Dielectric properties were
713 assigned based on the IT'IS Tissue Properties Database v4.0[105]. Rectilinear discretization was
714 performed, and grid convergence as well as solver convergence analyses were used to ensure
715 negligible numerical uncertainty, resulting in a grid that included more than 54M voxels. Dirichlet
716 voltage boundary conditions, and then current normalization were applied. The electrode-head
717 interface contact was treated as ideal. tTIS exposure was quantified according to the maximum
718 modulation envelope magnitude formula from Grossman et al., (2017)[40]. Then, a sweep over 960
719 permutations of the four electrode positions was performed, considering symmetric and
720 asymmetric montages with parallel (sagittal and coronal) or crossing current paths, while

721 quantifying bilateral striatum (putamen, caudate and nucleus accumbens) exposure performance
722 according to three metrics: a) target exposure strength, b) focality ratio (the ratio of target tissue
723 volume above threshold compared to the whole-brain tissue volume above threshold, a measure
724 of stimulation selectivity), and c) activation ratio (percentage of target volume above threshold with
725 respect to the total target volume, a measure of target coverage). We defined the threshold as the
726 98th volumetric iso-percentile level of the tTIS. From the resulting Pareto-optimal front, two
727 configurations stood out particularly: one that maximised focality and activation (AF3 - AF4, P7 -
728 P8) and a second one that accepts a reduction of these two metrics by a quarter, while increasing
729 the target exposure strength by more than 50% (F3-F4, TP7-TP8). This last montage was
730 selected, to ensure sufficient tTIS exposure in the striatum[51] (Figure 1C, 1D).

731

732 4.2.2.5. Electrode positioning and evaluation of stimulation-associated sensations

733

734 Based on the modelling approach described above, we defined the stimulation electrode
735 positions in the framework of the EEG 10-10 system[106]. The optimal montage leading in terms of
736 target (i.e. the bilateral striatum) exposure strength and selectivity, was composed of the following
737 electrodes: F3, F4, TP7 and TP8. Their locations were marked with a pen on the scalp and, after
738 skin preparation (cleaned with alcohol), round conductive rubber electrodes of 3 cm^2 were placed
739 adding a conductive paste (*Ten20, Weaver and Company, Aurora, CO, USA or Abralyt HiCl,*
740 *Easycap GmbH, Woerthsee-Etterschlag, Germany*) as an interface to the skin. Electrodes were
741 held in position with tape and cables were oriented towards the top in order to allow good
742 positioning inside the scanner. Impedances were checked and optimised until they were below 20
743 kΩ [47]. Once good contact was obtained, we tested different intensities of stimulation for each
744 stimulation protocol in order to familiarise the participants with the perceived sensations and to
745 systematically document them. $tTIS_{Sham}$, $tTIS_{20Hz}$ and $tTIS_{80Hz}$ were applied for 20 seconds with the
746 following increasing current amplitudes per channel: 0.5 mA, 1 mA, 1.5 mA and 2 mA. Participants

747 were asked to report any kind of sensation and, if a sensation was felt, they were asked to grade
748 the intensity from 1 to 3 (light to strong) as well as give at least one adjective to describe it (Figure
749 S2). Following this step, cables were removed to be replaced by MRI-compatible cables and a
750 bandage was added to apply pressure on the electrodes and keep them in place. An impedance
751 check was repeated in the MRI right before the training and after the intervention.

752
753 4.2.3. MRI data acquisition
754
755 Structural and functional images were acquired using a 3T MAGNETOM PRISMA scanner
756 (*Siemens, Erlangen, Germany*). T1-weighted images were acquired via the 3D MPRAGE
757 sequence with the following parameters: TR = 2.3 s; TE = 2.96 ms; flip angle = 9°; slices = 192;
758 voxel size = 1 × 1 × 1 mm, FOV = 256 mm. Anatomical T2 images were also acquired with the
759 following parameters: TR = 3 s; TE = 409 ms; flip angle = 120°; slices = 208; voxel size = 0.8 ×
760 0.8 × 0.8 mm, FOV = 320 mm. Finally, functional images were recorded using Echo-Planar
761 Imaging (EPI) sequences with the following parameters: TR = 1.25 s; TE = 32 ms; flip angle =
762 58°; slices = 75; voxel size = 2 × 2 × 2 mm; FOV = 112 mm.

763

764 **4.3. Data and statistical analyses**
765
766 Data and statistical analyses were carried out with Matlab 2018a (the Mathworks, Natick,
767 Massachusetts, USA) and the R software environment for statistical computing and graphics (R
768 Core Team 2021, Vienna, Austria). Robust linear regressions were fitted with the Matlab function
769 robustfit. Linear mixed models (LMM) were fitted using the lmer function of the lme4 package in R
770 [107]. As random effects, we added intercepts for participants and block. Normality of residuals, and
771 homoscedasticity of the data were systematically checked, and logarithmic transformations were
772 applied when necessary (i.e., when skewness of the residuals' distribution was not comprised

773 between - 2 and 2[108] or when homoscedasticity was violated based on visual inspection). To
774 mitigate the impact of isolated influential data points on the outcome of the final model, we used
775 tools of the influence.ME package to detect and remove influential cases based on the following
776 criterion: distance > 4 * mean distance[109]. Statistical significance was determined using the anova
777 function with Satterthwaite's approximations of the lmerTest package[110]. For specific post-hoc
778 comparisons we conducted pairwise comparisons by computing estimated marginal means with
779 the emmeans package with Tukey adjustment of p-values[111]. Effect size measures were obtained
780 using the effectsize package[112]. The level of significance was set at $p<0.05$.

781
782
783 4.3.1. Behavioural data
784
785 4.3.1.1. Evaluation of motor learning
786
787 The main goal of the present study was to evaluate the influence of striatal tTIS on
788 reinforcement motor learning. To do so, we first removed trials, in which participants did not react
789 within 1 s after the appearance of the cursor and target, considering that these extremely long
790 preparation times may reflect significant fluctuations in attention[113]. This occurred extremely rarely
791 (0.52 % of the whole data set). For each subject and each trial, we then quantified the tracking
792 Error as the absolute force difference between the applied and required force as done
793 previously[4,53,55]. Tracking performance during Training and Post-training trials were then
794 normalised according to subjects' initial level by expressing the Error data in percentage of the
795 average Pre-training Error for each block. In order to test our main hypothesis predicting specific
796 effects of striatal tTIS on reinforcement motor learning, we performed a LMM on the Post-training
797 data with $tTIS_{TYPE}$ and $Reinf_{TYPE}$ as fixed effects. We then also ran the same analysis on the
798 Training data, to evaluate if striatal tTIS also impacted on motor performance, while stimulation
799 was being delivered.

As a control, we checked that initial performance at Pre-training was not different between conditions with a LMM on the Error data obtained at Pre-training. Again, $tTIS_{TYPE}$ and $Reinf_{TYPE}$ were considered as fixed effects. Finally, another LMM was fitted with the fixed effect $tTIS_{TYPE}$ to verify that the amount of positive reinforcement (as indicated by a green target) in the $Reinf_{ON}$ blocks was similar across $tTIS_{TYPES}$.

4.3.2. fMRI data

4.3.2.1. Imaging Preprocessing

We analyzed functional imaging data using Statistical Parametric Mapping 12 (*SPM12; The Wellcome Department of Cognitive Neurology, London, UK*) implemented in MATLAB R2018a (*Mathworks, Sherborn, MA*). All functional images underwent a common preprocessing including the following steps: slice time correction, spatial realignment to the first image, normalization to the standard MNI space and smoothing with a 6 mm full-width half-maximal Gaussian kernel. T1 anatomical images were then co-registered to the mean functional image and segmented. This allowed to obtain bias-corrected gray and white matter images, by normalizing the functional images via the forward deformation field. To select subjects with acceptable level of head movement, framewise displacement was calculated for each run. A visual check of both non-normalised and normalised images was performed in order to ensure good preprocessing quality. Finally, possible tTIS-related artifacts were investigated based on signal to noise ratio maps (see below).

4.3.2.2. Signal to Noise Ratio

Total signal to noise ratio (tSNR) maps were computed to check the presence of possible artifacts induced by the electrical stimulation. The values were calculated as mean over standard

827 deviation of each voxel time series. Spherical regions of interest were then defined both
828 underneath the tTIS electrodes and at 4 different locations, distant from the electrodes as a
829 control. The center of each spherical ROI was obtained by projecting the standard MNI
830 coordinates on the scalp[114] toward the center of the brain. After visual inspection of the ROIs,
831 average tSNR maps were extracted and a LMM was used to compare signal to noise ratio
832 underneath the electrodes and in the control regions. The results of this analysis are presented in
833 Supplementary materials (Figure S5).

834

835 4.3.2.3. Task-based BOLD activity analysis

836

837 A general linear model was implemented at the single-subject level in order to estimate
838 signal amplitude. Eight regressors were included in the model: 6 head motion parameters
839 (displacement and rotation) and normalised time series within the white matter and the
840 corticospinal fluid. Linear contrasts were then computed to estimate specific activity during the
841 motor task with respect to resting periods. Functional activation was also extracted within specific
842 ROIs individually defined based on structural images. More specifically, the Freesurfer recon-all
843 function was run based on the structural T1w and T2w images
844 (*https://surfer.nmr.mgh.harvard.edu/*). The BNA parcellation was derived on the individual subject
845 space and the selected ROIs were then co-registered to the functional images and normalised to
846 the MNI space. BOLD activity within the individual striatal masks was averaged and compared
847 between different striatal nuclei namely the putamen, caudate and NAc. Comparison between
848 conditions were presented for uncorrected voxel-wise FWE, p=0.001 and multiple comparison
849 corrected at the cluster level to reduce False Discovery Rate (FDR), p=0.05.

850

851

4.3.2.4. Effective connectivity analyses

As an additional investigation, we computed task-modulated effective functional connectivity by means of the CONN toolbox 2021a (www.nitrc.org/projects/conn, RRID:SCR_009550) running in Matlab R2018a (*Mathworks, Sherborn, MA*). An additional denoising step was added by applying a band-pass filtering from 0.01 to 0.1 Hz and by regressing potential confounders (white matter, CSF and realignment parameters). After that, generalized Psycho-Physiological Interactions (gPPI) connectivity was extracted within specific pre-defined customised sub-networks: a reward and a motor network. The reward network was defined as following: two regions within the striatum, namely the NAc (BNA regions 223 and 224) and the ventro-medial putamen (BNA regions 225 and 226, left and right respectively), and two frontal areas, namely the anterior cingulate (BNA regions 177, 179, 183 and 178, 180, 184, left and right respectively) and the orbitofrontal cortex within the vmPFC (BNA regions 41, 45, 47, 49, 187 and 42, 46, 48, 50, 188 for left and right respectively). The motor network included the following areas: the medial part of the SMA (BNA regions 9 and 10, left and right respectively) and the part of the M1 associated to upper limb function (BNA regions 57 and 58, left and right respectively). Notably, we considered connectivity in the left and right motor and reward networks regardless of laterality. Finally, gPPI was also extracted within a control language network, defined based on the functional atlas described by Shirer et al.(2012)[72].

Supplementary material

1. Exclusion criteria

- Unable to consent
- Severe neuropsychiatric (e.g., major depression, severe dementia) or unstable systemic diseases (e.g., severe progressive and unstable cancer, life threatening infectious diseases)
- Severe sensory or cognitive impairment or musculoskeletal dysfunctions prohibiting to understand instructions or to perform the experimental tasks
- Color blindness
- Inability to follow or non-compliance with the procedures of the study
- Contraindications for NIBS or MRI:
    - Electronic or ferromagnetic medical implants/device, non-MRI compatible metal implant
    - History of seizures
    - Medication that significantly interacts with NIBS being benzodiazepines, tricyclic antidepressant and antipsychotics
- Regular use of narcotic drugs
- Left-handedness
- Pregnancy
- Request of not being informed in case of incidental findings
- Concomitant participation in another trial involving probing of neuronal plasticity.

2. ContES Checklist

Technological factors	
Manufacturer of Stimulator	DS5 Isolated Bipolar Constant Current Stimulator (Digitimer)
MR Conditional Electrode Details	Round, 3 cm2 conductive rubber electrodes
Electrode Positioning	F3 → F4 TP7 → TP8 A bandage is warped around the head to apply pressure and keep the electrodes in place Electrodes are oriented in order to have vertical cables entering parallel to the MRI coil Head was fixed with pillows to avoid movements
MR Conditional Skin-Electrode Interface	10-20 gel One or two drops of saline were added when impedances were too high
Amount of Contact Medium (Paste/Gel/Electrolyte)	Around 1mm of paste was manually placed on the electrodes
Electrode Placement Visualization	Pictures 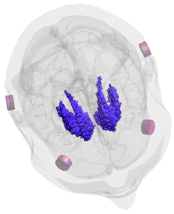

RF Filter	NeuroConn DC-STIMULATOR MR RF filter module with MRI-compatible cables and electrodes
Wire Routing Pattern	10 m ethernet cables between inner and outer box pass through a conduit along the wall of the MRI room until reaching the back of the MRI. Cables are then fixed with straps on the ground and on the wall of the MRI machine in order to avoid loops until reaching the interior of the coil. Cables between the head and the inner boxes were also fixed with straps and they were oriented in order to exit the magnetic field direction as soon as possible as indicated by the red arrows of the image below. 
tES-fMRI Machine Synchronization/Communication	Stimulation was triggered by the stimulus delivery PC via parallel port to BNC cable. The parallel port of the stimulus delivery PC was connected to the DAQ controlling the stimulators. Stimulus delivery PC, in turn, was also receiving the scanner trigger from the scanner via USB port.
Safety and noise tests	
MR Conditionality Specifics for tES Setting	Please refer to Section “Methods-Imaging acquisition”
tES-fMRI Setting Test - Safety Testing	Impedances were checked before and after

	the stimulation. No temperature tests were performed during the experiment. Intensity titration was performed prior to entering the MRI, testing increasing currents (0.5, 1, 1.5 and 2 mA) and asking the subject to report any type of sensation. A sensation questionnaire was also performed at the end of the experiment.
tES-fMRI Setting Test - Subjective Intolerance Reporting	No intolerances were reported by any subject
tES-fMRI Setting Test - Noise/Artifact	Signal to Noise Ratio (SNR) analysis was performed on the fMRI images, please refer to Section “Methods-Signal to Noise Ratio”
Impedance Testing	Impedances were checked right after electrodes positioning outside the scanner, before and after the stimulation inside. One or two drops of saline solution were added if impedances were higher than 20kΩ
Methodological factors	
Concurrent tES-fMRI Timing	For timings, please refer to the “Methods-Stimulation protocols” section To mitigate the impact of potential carry-over effects on our experimental results we used the following strategy: 1) We stimulated for short periods in each condition (5 minutes interspersed with resting periods without stimulation; see “Methods-Stimulation protocols”); 2) We imposed breaks (~7-8 minutes) between each stimulation protocol; 3) We randomised the order of the

	Stimulation conditions
Imaging Session Timing	All sequences were performed with TI stimulation electrodes placed on the subjects' head.
tES Experience Report	Please refer to "Results" section and to Figure S2.

Table S1. ContES checklist as recommended in Ekhtiari et al., 2022 for concurrent tES-fMRI studies.

3. Patterns of motion of the target used in the study

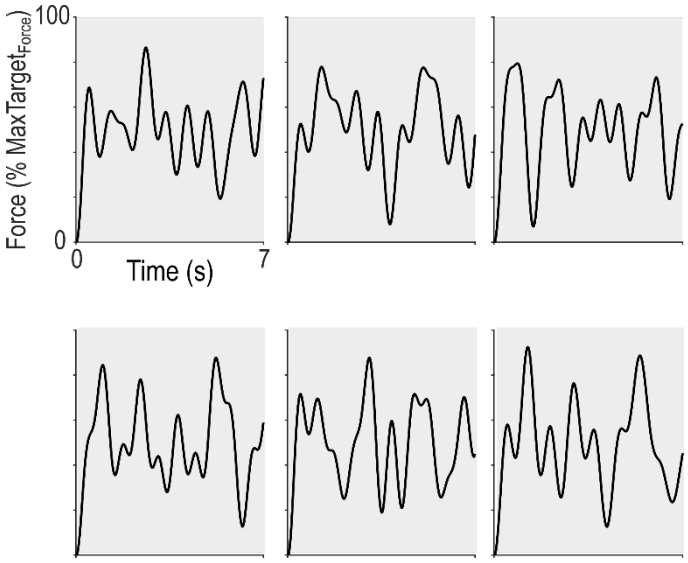

Figure S1. Patterns of motion of the target. For each block of training, participants had to learn a new pattern of motion of the target. The patterns had similar mathematical properties and their relationship to a condition was randomised (see Methods for more details)..

4. Control analyses of behavioural data

Pre-training performance

In order to verify that our main behavioural results were not influenced by potential differences in initial performance between conditions despite randomization, we analysed the Error at Pre-training between conditions. We did not find any $tTIS_{TYPE}$ ($F_{(2,519.15)}$=1.64; p=0.20) or $tTIS_{TYPE}$ x $Reinf_{TYPE}$ effect ($F_{(2,519.99)}$=1.08; p=0.34), suggesting that the main behavioural results

could not be accounted for by differences in initial performance between conditions. However, the LMM did reveal a $Reinf_{TYPE}$ effect ($F_{(1,519.15)}$=12.47; p<0.001), that was due to the fact that Pre-training performance was generally better in $Reinf_{OFF}$ blocks. This effect, which was opposite to our learning results (generally better learning with $Reinf_{ON}$), may be related to an expectancy effect stemming from the repetitive structure of the reinforcement conditions (see Methods). However, the absence of interaction with $tTIS_{TYPE}$ is strongly suggestive that this effect did not drive any of the main findings. Put together, these data provide confidence that the differential effects of striatal tTIS on motor learning depending on the presence of reinforcement were not the result of different initial performance between conditions.

Success rate

Overall, the amount of positive reinforcement (i.e., when the target was green) averaged 52.78 +/- 0.42% and was comparable across $tTIS_{TYPES}$ ($F_{(2,1702)}$=0.17; p=0.84), suggesting that the closed-loop reinforcement schedule was successful at providing similar reinforcement feedback despite differences in performance between conditions. Hence, different success rates during training cannot explain the effect of the different striatal tTIS conditions on motor learning.

Frequency of flashing

Analysis of the frequency of flashing in the different conditions did not reveal any effect of $tTIS_{TYPE}$ ($F_{(2,3283)}$=0.85; p=0.43) nor any $Reinf_{TYPE}$ x $tTIS_{TYPE}$ interaction ($F_{(2,3283)}$=0.19; p=0.82), suggesting that the behavioural effects of tTIS could not be explained by a visual confound. However, this analysis did reveal a $Reinf_{TYPE}$ effect ($F_{(1,3283)}$=33.62; p<0.001) which was due to the fact that the average frequency in the $Reinf_{OFF}$ condition (4.28 ± 0.097 Hz) was slightly but significantly higher than with $Reinf_{ON}$ (4.08 ± 0.098 Hz; $F_{(1,3283)}$=33.62; p<0.001). Notably, in absolute terms, this difference represented only a difference of 1.4 change of color over the whole

7 s trial, which we think is unlikely to explain the improvement of performance in the $Reinf_{ON}$ condition.

5. Blinding integrity and tTIS-evoked sensations

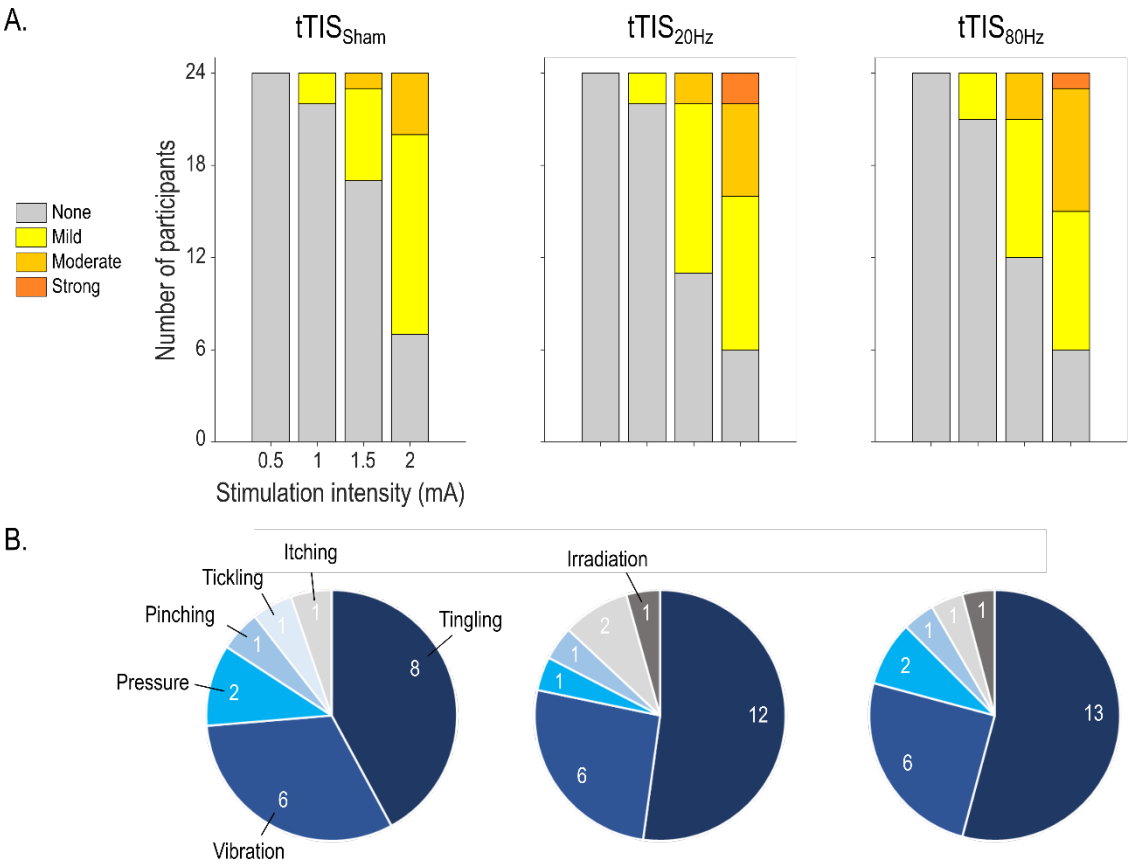

Figure S2. tTIS-related sensations. A) Magnitude of tTIS-related sensations. Magnitude of sensations reported before the experiment for current amplitudes ranging from 0.5 to 2 mA for each $tTIS_{TYPE}$. The current amplitude used in the present experiment was 2 mA. **B) Types of tTIS-related sensations.** Type of sensations as described by the participants, at 2 mA. Note that subjects were allowed to describe their sensations with up to two different words.

6. Brain activity during reinforcement motor learning

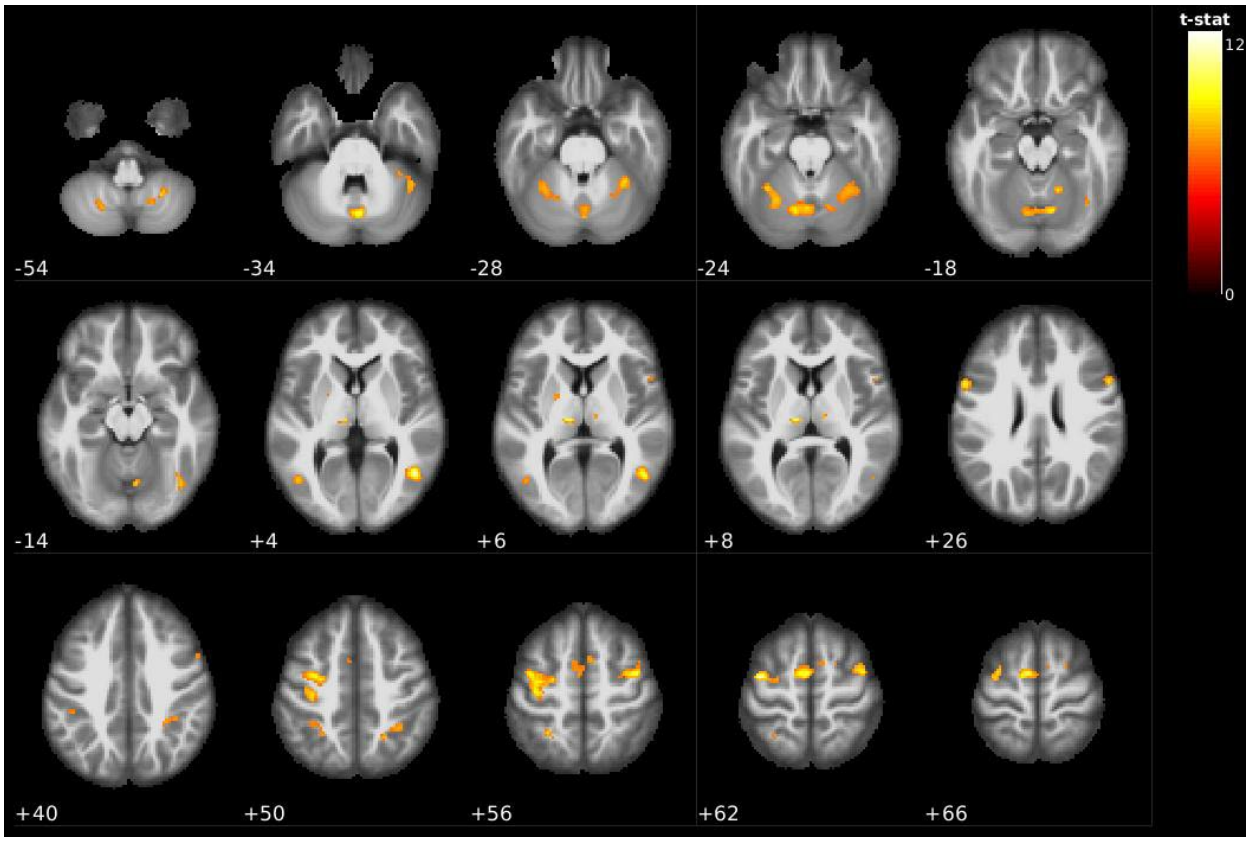

Figure S3. Whole-brain activity during reinforcement motor learning. Activation maps for the contrast task>rest in the $tTIS_{Sham}$, $Reinf_{ON}$ condition showing activation of key areas of the reinforcement motor learning network including the putamen, thalamus, cerebellum and sensorimotor network, especially on the left side. Significant clusters are shown for corrected voxel-wise family wise error (FWE), p=0.05, and corrected cluster-based false discovery rate (FDR), p=0.05.

Cluster-level				Peak-level					x	y	z	Region
$p_{FWE-corr}$	$q_{FDR-corr}$	k_E	P_{uncorr}	$p_{FWE-corr}$	$q_{FDR-corr}$	T	(Z_E)	P_{uncorr}				
<0.001	<0.001	135	<0.001	<0.001	0.005	12.63	6.84	<0.001	46	-62	4	Temporal_Mid_R
<0.001	<0.001	523	<0.001	<0.001	0.005	12.32	6.77	<0.001	-40	-8	62	Precentral_L
				<0.001	0.021	10.62	6.33	<0.001	-34	-6	52	Postcentral_L
				<0.001	0.021	10.43	6.28	<0.001	-36	-20	54	Precentral_L
<0.001	<0.001	335	<0.001	<0.001	0.018	11.08	6.46	<0.001	-8	-6	64	Supp_Motor_Area_L
				0.003	0.145	8.21	5.56	<0.001	6	6	58	Supp_Motor_Area_R
				0.003	0.145	8.20	5.55	<0.001	-4	-2	54	Supp_Motor_Area_L
<0.001	<0.001	44	<0.001	<0.001	0.021	10.65	6.34	<0.001	-10	-20	6	Thal_IL_L
<0.001	<0.001	162	<0.001	<0.001	0.021	10.36	6.26	<0.001	42	-6	56	Frontal_Mid_2_R
				<0.001	0.042	9.48	5.99	<0.001	34	-4	58	Frontal_Sup_2_R
<0.001	<0.001	175	<0.001	<0.001	0.021	10.27	6.23	<0.001	-58	10	28	Precentral_L
				<0.001	0.037	9.60	6.03	<0.001	-56	8	20	Frontal_Inf_Oper_L
				0.019	0.490	7.32	5.21	<0.001	-48	2	16	Rolandic_Oper_L
<0.001	<0.001	601	<0.001	<0.001	0.024	10.06	6.17	<0.001	2	-74	-34	Vermis_7
				<0.001	0.025	9.99	6.15	<0.001	-12	-70	-22	Cerebellum_6_L
				<0.001	0.027	9.88	6.12	<0.001	12	-70	-20	Cerebellum_6_R
<0.001	<0.001	82	<0.001	<0.001	0.070	9.14	5.88	<0.001	56	10	26	Frontal_Inf_Oper_R
				0.006	0.234	7.86	5.42	<0.001	56	10	38	Precentral_R
<0.001	<0.001	141	<0.001	0.001	0.092	8.89	5.80	<0.001	-34	-52	-24	Cerebellum_6_L
				0.002	0.117	8.47	5.65	<0.001	-28	-62	-24	Cerebellum_6_L
<0.001	<0.001	76	<0.001	0.001	0.092	8.87	5.79	<0.001	-28	-52	56	Parietal_Sup_L
				0.011	0.341	7.57	5.31	<0.001	-30	-44	48	Parietal_Inf_L
<0.001	<0.001	200	<0.001	0.001	0.092	8.77	5.76	<0.001	32	-48	-28	Cerebellum_6_R
				0.013	0.382	7.49	5.28	<0.001	34	-40	-34	Cerebellum_6_R
<0.001	<0.001	36	<0.001	0.001	0.092	8.73	5.74	<0.001	16	-54	-18	Cerebellum_4_5_R
<0.001	<0.001	28	<0.001	0.001	0.101	8.63	5.71	<0.001	26	-58	-54	Cerebellum_8_R
<0.001	<0.001	62	<0.001	0.001	0.113	8.51	5.67	<0.001	38	-62	-16	Fusiform_R
				0.002	0.117	8.45	5.64	<0.001	42	-72	-12	Occipital_Inf_R
<0.001	<0.001	21	<0.001	0.002	0.117	8.41	5.63	<0.001	-46	-68	4	Occipital_Mid_L
<0.001	<0.001	141	<0.001	0.002	0.130	8.33	5.60	<0.001	22	-56	50	Location not in atlas
				0.002	0.130	8.30	5.59	<0.001	30	-48	48	Parietal_Sup_R
				0.007	0.266	7.76	5.39	<0.001	36	-40	42	SupraMarginal_R
<0.001	<0.001	29	<0.001	0.004	0.170	8.09	5.51	<0.001	44	-50	-34	Cerebellum_Crus1_R

<0.001	<0.001	59	<0.001	0.004	0.178	8.04	5.49	<0.001	-22	-66	-52	Cerebellum_8_L
<0.001	0.006	12	0.003	0.004	0.190	7.99	5.47	<0.001	10	-16	8	Thal_MDl_R
0.001	0.043	6	0.028	0.009	0.319	7.63	5.33	<0.001	-22	-2	6	Putamen_L
<0.001	<0.001	34	<0.001	0.009	0.319	7.63	5.33	<0.001	18	-64	-54	Cerebellum_8_R
0.001	0.300	7	0.019	0.023	0.545	7.23	5.17	<0.001	20	2	62	Frontal_Sup_2_R
0.001	0.030	7	0.019	0.024	0.560	7.21	5.16	<0.001	52	12	8	Frontal_Inf_Oper_R
0.001	0.030	7	0.019	0.025	0.568	7.19	5.16	<0.001	-44	-36	40	Parietal_Inf_L

Table S2: Significant clusters and the respective local maxima in the $tTIS_{Sham}$, $Reinf_{ON}$ condition. Related to Figure S3. Regions were identified with the Automated Anatomical Labelling atlas 3 (AAL3, Rolls et al., 2020). Significant clusters were selected for corrected voxel-wise family wise error (FWE), p=0.05, and corrected cluster-based false discovery rate (FDR), p=0.05.

7. Correlation between effect of $tTIS_{80Hz}$ on reinforcement motor learning and modulation of whole-brain activity

Cluster-level				Peak-level					x	y	z	Region
$p_{FWE-corr}$	$q_{FDR-corr}$	k_E	P_{uncorr}	$p_{FWE-corr}$	$q_{FDR-corr}$	T	(Z_E)	P_{uncorr}				
0.003	**0.005**	**157**	**<0.001**	**0.027**	**0.065**	**7.29**	**5.14**	**<0.001**	**10**	**18**	**0**	Caudate_R
				0.639	0.678	5.38	4.25	<0.001	0	0	10	Location not in atlas
				0.921	0.757	4.89	3.98	<0.001	6	6	2	Location not in atlas
0.007	**0.005**	**138**	**<0.001**	**0.693**	**0.678**	**5.30**	**4.21**	**<0.001**	**-16**	**14**	**6**	Location not in atlas
				0.923	0.757	4.88	3.98	<0.001	-22	14	-2	Putamen_L
				1.000	0.810	4.26	3.60	<0.001	-18	8	-6	Putamen_L

Table S3. Significant clusters for the correlation between the behavioural and neural effects of $tTIS_{80Hz}$ (vs. $tTIS_{20Hz}$). Related to Figure 3B. Two significant clusters were found with several local maxima. Notably, the left cluster also encompassed a portion of the left caudate (related to Figure 3). Regions were identified with the Automated Anatomical Labelling atlas 3 (AAL3[115]). Significant clusters were selected for uncorrected voxel-wise family wise error (FWE), p=0.001, and corrected cluster-based false discovery rate (FDR), p=0.05.

8. Relationship between the neural and behavioural effects of $tTIS_{80Hz}$ and impulsivity

Characterising individual factors that influence responsiveness to brain stimulation is an important line of research both for fundamental neuroscience but also to determine profiles of responders for future clinical translation. Based on previous literature linking striatal gamma

oscillatory mechanisms and impulsivity[74], we explored the possibility that impulsivity influences responsiveness to striatal $tTIS_{80Hz}$ (**Figure S4**).

First, we exploited the BOLD data and asked if inter-individual variability in the neural effects of $tTIS_{80Hz}$ during reinforcement motor learning (i.e., in the $Reinf_{ON}$ condition) was related to impulsivity at the whole-brain level. Impulsivity was evaluated by a well-established independent delay-discounting questionnaire performed at the beginning of the experiment[77,78]. Strikingly, this analysis revealed that impulsivity was associated to the effect of $tTIS_{80Hz}$ (with respect to $tTIS_{20Hz}$) specifically in the left caudate nucleus (Figure S4A, Table S4). No other clusters were found. As such, the most impulsive participants exhibited an increase of left caudate activity with $tTIS_{80Hz}$ (compared to $tTIS_{20Hz}$) while the least impulsive ones rather presented a decrease of BOLD signal, consistent with the idea that impulsivity modulates the neuronal responsiveness to tTIS (R^2=0.47; $p<0.001$; Figure S4B). No significant clusters of correlation were found for the $tTIS_{80Hz} - tTIS_{Sham}$ contrast, neither for the control $tTIS_{20Hz} - tTIS_{Sham}$ contrast. Hence, this analysis suggests that the effect of $tTIS_{80Hz}$ on caudate activity depends on participants' impulsivity.

As a second step, we aimed at evaluating the association between impulsivity and the increased striatum to motor cortex connectivity observed with $tTIS_{80Hz}$, in the presence of reinforcement. Notably, such pattern of hyper-connectivity in fronto-striatal circuits has been described as a pathophysiological mechanism in multiple neuro-psychiatric disorders involving impulsivity[116–119]. Hence, we first asked if striatum to motor cortex connectivity was related to impulsivity during reinforcement motor learning in the absence of stimulation (i.e., in the $tTIS_{Sham}$ condition). Indeed, we found a significant positive relationship between impulsivity and striatum to motor cortex connectivity (robust linear regression: R^2=0.10; p=0.0038), in line with previous results[116–119]. Then, we evaluated whether the increase of connectivity observed with $tTIS_{80Hz}$ in the $Reinf_{ON}$ condition (Figure 4A) could be related to impulsivity. Indeed, we found that the effect of $tTIS_{80Hz}$ on connectivity was negatively correlated to impulsivity both when contrasting $tTIS_{80Hz}$

with $tTIS_{Sham}$ (R^2=0.19; p=0.043, Figure S4C, left) and with $tTIS_{20Hz}$ (R^2=0.28; p=0.021, Figure S4C, middle): participants with the largest increase in connectivity with $tTIS_{80Hz}$ in the $Reinf_{ON}$ condition were also the least impulsive ones. Such correlation was absent when contrasting $tTIS_{20Hz}$ and $tTIS_{Sham}$ (R^2=0.0031; p=0.31, Figure S4C, right), but also when considering the same contrasts in the reward instead of the motor network (p=0.93 and p=0.86 for the $tTIS_{80Hz}$-$tTIS_{Sham}$ and $tTIS_{80Hz}$-$tTIS_{20Hz}$ contrasts, respectively). Hence, striatum to motor cortex effective connectivity during the task was positively correlated to impulsivity, but the change in connectivity induced by $tTIS_{80Hz}$ was rather negatively associated with impulsivity. This may be due to a ceiling effect in the most impulsive participants: exhibiting initially high levels of connectivity may leave less room for further modulation by $tTIS_{80Hz}$. These results suggest that inter-individual variability in impulsivity might influence neural responses to striatal $tTIS_{80Hz}$.

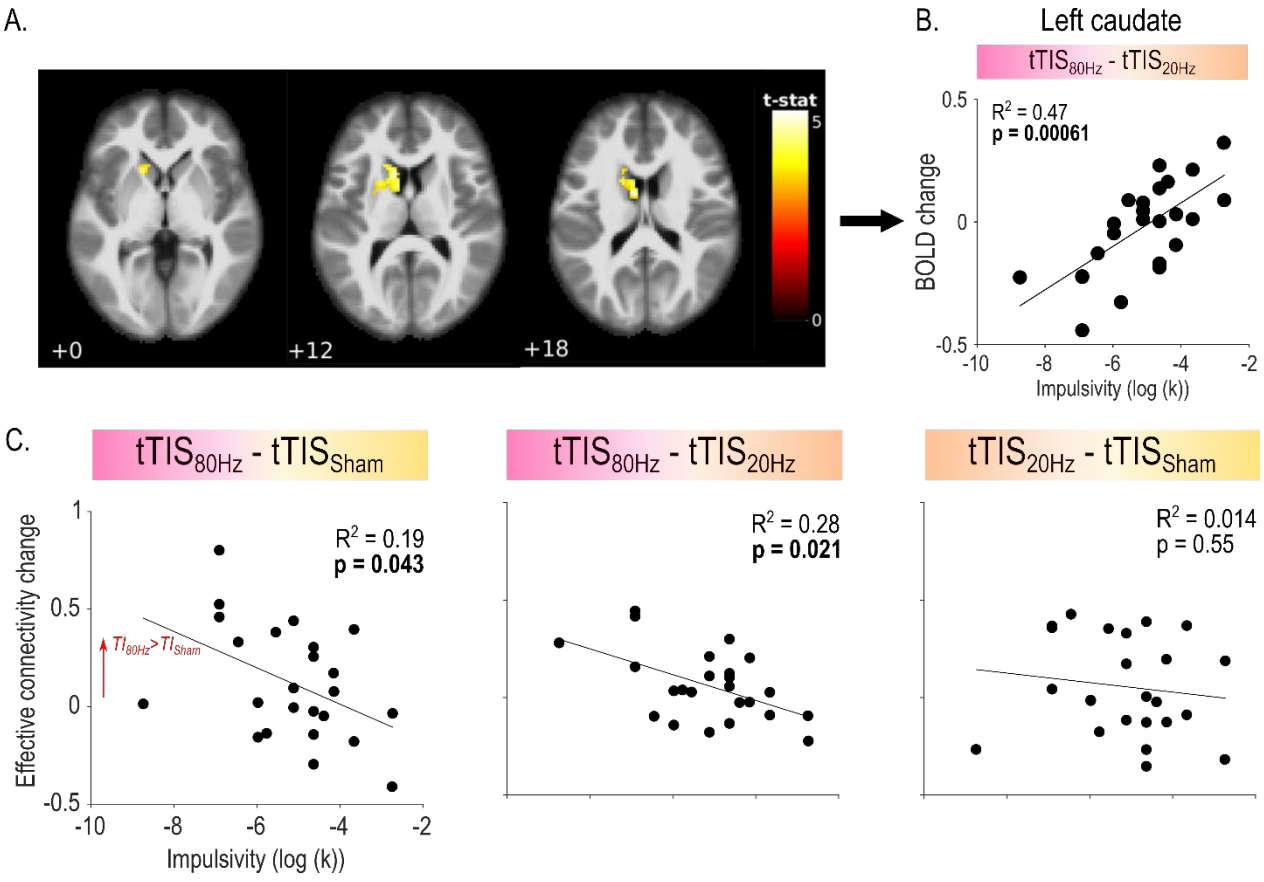

Figure S4. Relationship between impulsivity and the neural effects of $tTIS_{80Hz}$. A) Whole-brain correlation between the neural effects of $tTIS_{80Hz}$ (with respect to $tTIS_{20Hz}$) and impulsivity. Correlation between tTIS-related modulation of striatal activity ($tTIS_{80Hz} - tTIS_{20Hz}$) during reinforcement motor learning ($Reinf_{ON}$) and individual impulsivity levels. A single significant cluster of correlation was found in left caudate (uncorrected voxel-wise FWE: p=0.001, and corrected cluster-based FDR: p=0.05). **B) Correlation between left caudate activity and impulsivity.** A positive correlation was found showing that participants with higher levels of impulsivity exhibited stronger activation of the left caudate in the $tTIS_{80Hz}$ (with respect to $tTIS_{20Hz}$). **C) Correlations between impulsivity and tTIS-related modulation of effective connectivity.** Impulsivity was associated to the neural effects of $tTIS_{80Hz}$ both when contrasting to $tTIS_{Sham}$ (left) and $tTIS_{20Hz}$ (middle), but was not correlated to the effect of $tTIS_{20Hz}$ (right).

Cluster-level				Peak-level					x	y	z	Region
$p_{FWE-corr}$	$q_{FDR-corr}$	k_E	P_{uncorr}	$p_{FWE-corr}$	$q_{FDR-corr}$	T	(Z_E)	P_{uncorr}				
<0.001	**<0.001**	**254**	**<0.001**	**0.707**	**0.524**	**5.29**	**4.20**	**<0.001**	**-8**	**0**	**18**	Location not in atlas
				0.719	0.524	5.27	4.19	<0.001	-14	16	16	Caudate_L
				0.971	0.620	4.72	3.88	<0.001	-16	16	0	Location not in atlas

Table S4. Significant clusters for the correlation between impulsivity and effects of $tTIS_{80Hz}$ on BOLD activity (vs. $tTIS_{20Hz}$). Related to Figure S4A. One significant cluster encompassing the left caudate nucleus was found. Regions were identified with AAL3[115].

As a last step, we verified if impulsivity was also predictive of the behavioural effects of $tTIS_{80Hz}$ on reinforcement motor learning. We did not find any significant correlation between impulsivity and the effect of $tTIS_{80Hz}$ on motor learning ($tTIS_{80Hz} - tTIS_{Sham}$: R^2=0.098; p=0.17; $tTIS_{80Hz} - tTIS_{20Hz}$: R^2=0.11; p=0.21). Hence, impulsivity was associated to the neural, but not the behavioural effects of $tTIS_{80Hz}$.

9. Imaging quality control

A threshold of 0.5 was chosen to discard subjects showing more than 40% of voxels with framewise displacement FD higher than this threshold. In the current study cohort, no subject exceeded the limit value, thus the whole dataset could be used. Furthermore, successful cleaning

of the data was ensured by visual checking the preprocessing results. In particular, good registration between anatomical and functional images and normalization to standard space were checked.

Signal to noise ratio analysis showed significantly higher tSNR values underneath the stimulating electrodes ($F_{(1,1122)}$=249.25, p<0.001; **Figure S5**). This result suggests that the stimulation did not introduce additional noise to the MR images. In summary, all controls confirmed the good quality of the imaging data.

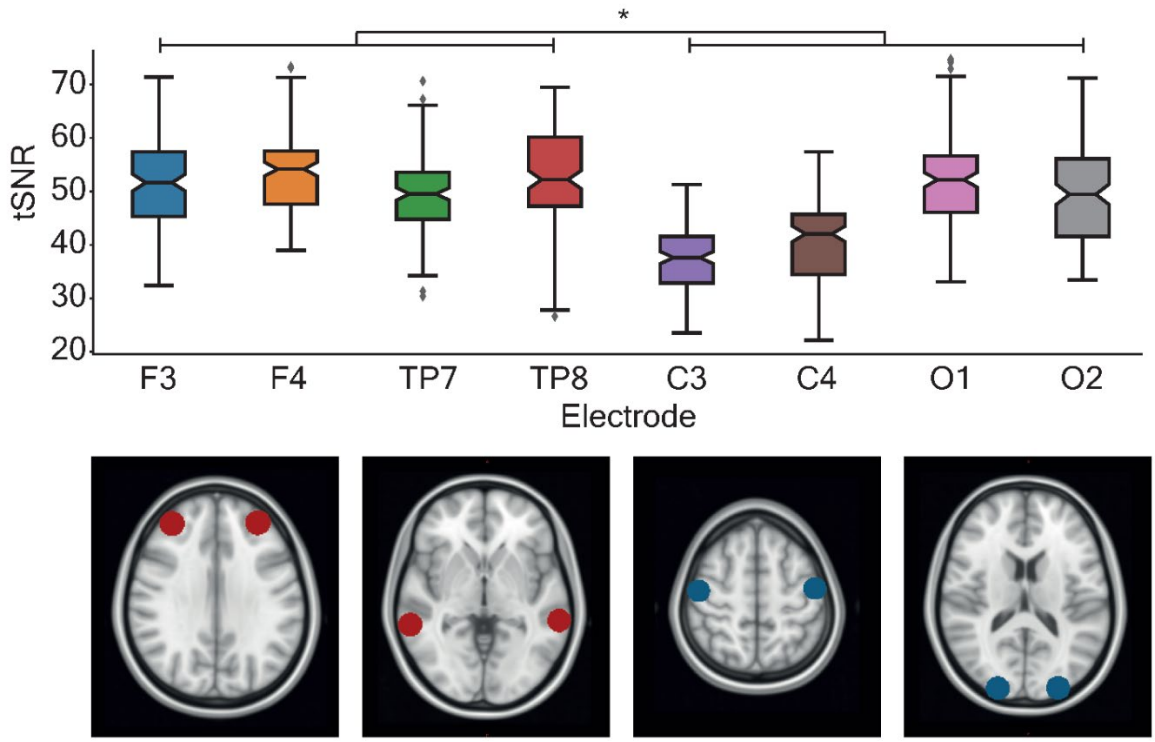

Figure S5. Total signal to noise ratio (tSNR). Total signal to noise ratio investigation. On the top panel, the average tSNR is shown within spheres of 10mm radius underneath the 4 stimulation electrodes (F3, F4, TP7 and TP8) and underneath other 4 locations more distal from the electrodes (C3, C4, O1 and O2). A significant higher tSNR was found underneath the electrodes with respect to the distal locations ($F_{(1,1122)}$=249.25, p<0.001). This indicates that there was no reduction of the tSNR due to the presence of electrical current. On the bottom panel, the location of the spheres from where the average tSNRs were extracted: F3 and F4 in red in the first image from the left, TP7 and TP8 in red on the second image from the left, C3 and C4 in blue on the third image from the left, O1 and O2 in blue on the forth image from the left.

Acknowledgements

P.V. was a PhD student supported by the Fund for Research training in Industry and Agriculture (FRIA/FNRS; FC29690), and grants by the Platform for Education and Talent (Gustave Boël - Sofina Fellowships) and Wallonie-Bruxelles International. J.D. was supported by grants from the Belgian FNRS and the Fondation Médicale Reine Elisabeth (FMRE). G.D. was supported by the Belgian FNRS. The research was partially funded by the Novartis Research Foundation—FreeNovation (Basel, CH) to MJW and EN, the Bertarelli Foundation (Catalyst 'Deep-MCI-T',Gstaad, CH) to FCH, the SNSF Lead Agency (NiBS-iCog 320030L_197899) to FCH and the Defitech Foundation (Morges, CH) to FCH. We acknowledge access to and expertise of the Neuromodulation and the Neuroimaging facilities of the Human Neuroscience Platform of the Campus Biotech Geneva and of the MRI Platform of the HVS (Sion). We would also like to thank Prof. Leonardo Cohen for insightful feedback on a previous version of this manuscript.

Competing interests

E.N. is co-founder of TI Solutions AG, a company committed to producing hardware and software solutions to support tTIS research.

References

1. Neftci, E. O. & Averbeck, B. B. Reinforcement learning in artificial and biological systems. *Nat. Mach. Intell.* **1**, 133–143 (2019).

2. Schultz, W. Neuronal Reward and Decision Signals: From Theories to Data. *Physiol. Rev.* **95**, 853–951 (2015).

3. Dhawale, A. K., Smith, M. A. & Ölveczky, B. P. The Role of Variability in Motor Learning. *Annu. Rev. Neurosci.* **40**, 479–498 (2017).

4. Vassiliadis, P. *et al.* Reward boosts reinforcement-based motor learning. *iScience* **24**, 102821 (2021).

5. Spampinato, D. & Celnik, P. Multiple Motor Learning Processes in Humans: Defining Their Neurophysiological Bases. *Neuroscientist* **27**, 246–267 (2021).

6. Huang, V. S., Haith, A., Mazzoni, P. & Krakauer, J. W. Rethinking Motor Learning and Savings in Adaptation Paradigms: Model-Free Memory for Successful Actions Combines with Internal Models. *Neuron* **70**, 787–801 (2011).

7. Galea, J. M., Mallia, E., Rothwell, J. & Diedrichsen, J. The dissociable effects of punishment and reward on motor learning. *Nat Neurosci* **18**, 597–602 (2015).

8. Therrien, A. S., Wolpert, D. M. & Bastian, A. J. Effective Reinforcement learning following cerebellar damage requires a balance between exploration and motor noise. *Brain* **139**, 101–114 (2016).

9. Vassiliadis, P., Derosiere, G. & Duque, J. Beyond Motor Noise : Considering Other Causes of Impaired Reinforcement Learning in Cerebellar Patients. *Eneuro* **6**, 1–4 (2019).

10. Widmer, M. *et al.* Reward During Arm Training Improves Impairment and Activity After Stroke: A Randomized Controlled Trial. *Neurorehabil. Neural Repair* **0**, 154596832110628 (2021).

11. Bartra, O., McGuire, J. T. & Kable, J. W. The valuation system: A coordinate-based meta-analysis of BOLD fMRI experiments examining neural correlates of subjective value. *Neuroimage* **76**, 412–427 (2013).

12. Hardwick, R. M., Rottschy, C., Miall, R. C. & Eickhoff, S. B. A quantitative meta-analysis and review of motor learning in the human brain. *Neuroimage* **67**, 283–297 (2013).

13. Haber, S. N. Corticostriatal circuitry. *Dialogues Clin. Neurosci.* **18**, 7–21 (2016).

14. Balleine, B. W., Delgado, M. R. & Hikosaka, O. The role of the dorsal striatum in reward and decision-making. *J. Neurosci.* **27**, 8161–8165 (2007).

15. Piray, P., den Ouden, H. E. M., van der Schaaf, M. E., Toni, I. & Cools, R. Dopaminergic modulation of the functional ventrodorsal architecture of the human striatum. *Cereb. Cortex* **27**, 485–495 (2017).

16. Hori, Y. *et al.* Ventral striatum links motivational and motor networks during operant-conditioned movement in rats. *Neuroimage* **184**, 943–953 (2019).

17. Wachter, T., Lungu, O. V., Liu, T., Willingham, D. T. & Ashe, J. Differential Effect of Reward and Punishment on Procedural Learning. *J. Neurosci.* **29**, 436–443 (2009).

18. Widmer, M., Ziegler, N., Held, J., Luft, A. & Lutz, K. Rewarding feedback promotes motor skill consolidation via striatal activity. in *Progress in Brain Research* **5**, 303–

323 (2016).

19. Berke, J. D. Fast oscillations in cortical-striatal networks switch frequency following rewarding events and stimulant drugs. *Eur. J. Neurosci.* **30**, 848–859 (2009).

20. van der Meer, M. A. A. *et al.* Integrating early results on ventral striatal gamma oscillations in the rat. *Front. Neurosci.* **4**, 1–12 (2010).

21. van der Meer, M. A. A. & Redish, A. D. Low and high gamma oscillations in rat ventral striatum have distinct relationships to behavior, reward, and spiking activity on a learned spatial decision task. *Front. Integr. Neurosci.* **3**, 1–19 (2009).

22. Dwiel, L. L., Khokhar, J. Y., Connerney, M. A., Green, A. I. & Doucette, W. T. Finding the balance between model complexity and performance: Using ventral striatal oscillations to classify feeding behavior in rats. *PLoS Comput. Biol.* **15**, 1–19 (2019).

23. Matsumoto, J. *et al.* Neuronal responses in the nucleus accumbens shell during sexual behavior in male rats. *J. Neurosci.* **32**, 1672–1686 (2012).

24. Kalenscher, T., Lansink, C. S., Lankelma, J. V. & Pennartz, C. M. A. Reward-associated gamma oscillations in ventral striatum are regionally differentiated and modulate local firing activity. *J. Neurophysiol.* **103**, 1658–1672 (2010).

25. Cohen, M. X. *et al.* Good vibrations: Cross-frequency coupling in the human nucleus accumbens during reward processing. *J. Cogn. Neurosci.* **21**, 875–889 (2009).

26. Sepe-Forrest, L., Carver, F. W., Quentin, R., Holroyd, T. & Nugent, A. C. Basal

ganglia activation localized in MEG using a reward task. *Neuroimage: Reports* **1**, 100034 (2021).

27. Herrojo-Ruiz, M. *et al.* Involvement of human internal globus pallidus in the early modulation of cortical error-related activity. *Cereb. Cortex* **24**, 1502–1517 (2014).

28. Jenkinson, N. & Brown, P. New insights into the relationship between dopamine, beta oscillations and motor function. *Trends Neurosci.* **34**, 611–618 (2011).

29. Brown, P. Abnormal oscillatory synchronisation in the motor system leads to impaired movement. *Curr. Opin. Neurobiol.* **17**, 656–664 (2007).

30. McCarthy, M. M. *et al.* Striatal origin of the pathologic beta oscillations in Parkinson's disease. *Proc. Natl. Acad. Sci. U. S. A.* **108**, 11620–11625 (2011).

31. Kondabolu, K. *et al.* Striatal cholinergic interneurons generate beta and gamma oscillations in the corticostriatal circuit and produce motor deficits. *Proc. Natl. Acad. Sci. U. S. A.* **113**, 3159–3168 (2016).

32. Williams, Z. M. & Eskandar, E. N. Selective enhancement of associative learning by microstimulation of the anterior caudate. *Nat. Neurosci.* **9**, 562–568 (2006).

33. Nakamura, K. & Hikosaka, O. Facilitation of saccadic eye movements by postsaccadic electrical stimulation in the primate caudate. *J. Neurosci.* **26**, 12885–12895 (2006).

34. Deng, Z. De, Lisanby, S. H. & Peterchev, A. V. Electric field depth-focality tradeoff in transcranial magnetic stimulation: Simulation comparison of 50 coil designs. *Brain Stimul.* **6**, 1–13 (2013).

35. Wagner, T. *et al.* Transcranial direct current stimulation: A computer-based human

model study. *Neuroimage* **35**, 1113–1124 (2007).

36. Nickchen, K. *et al.* Reversal learning reveals cognitive deficits and altered prediction error encoding in the ventral striatum in Huntington's disease. *Brain Imaging Behav.* **11**, 1862–1872 (2017).

37. Schmidt, L. *et al.* Disconnecting force from money: Effects of basal ganglia damage on incentive motivation. *Brain* **131**, 1303–1310 (2008).

38. Seymour, B. *et al.* Deep brain stimulation of the subthalamic nucleus modulates sensitivity to decision outcome value in Parkinson's disease. *Sci. Rep.* **6**, 1–12 (2016).

39. Atkinson-Clement, C. *et al.* Effects of subthalamic nucleus stimulation and levodopa on decision-making in Parkinson's disease. *Mov. Disord.* **34**, 377–385 (2019).

40. Grossman, N. *et al.* Noninvasive Deep Brain Stimulation via Temporally Interfering Electric Fields. *Cell* **169**, 1029-1041.e16 (2017).

41. Song, S., Zhang, J., Tian, Y., Wang, L. & Wei, P. Temporal Interference Stimulation Regulates Eye Movements and Neural Activity in the Mice Superior Colliculus. *Proc. Annu. Int. Conf. IEEE Eng. Med. Biol. Soc. EMBS* 6231–6234 (2021). doi:10.1109/EMBC46164.2021.9629968

42. Esmaeilpour, Z., Kronberg, G., Reato, D., Parra, L. C. & Bikson, M. Temporal interference stimulation targets deep brain regions by modulating neural oscillations. *Brain Stimul.* **14**, 55–65 (2021).

43. Rampersad, S. *et al.* Prospects for transcranial temporal interference stimulation

in humans: A computational study. *Neuroimage* **202**, 116124 (2019).

44. von Conta, J. *et al.* Interindividual variability of electric fields during transcranial temporal interference stimulation (tTIS). *Sci. Rep.* **11**, 1–12 (2021).

45. Cao, J., Doiron, B., Goswami, C. & Grover, P. The mechanics of temporal interference stimulation. *bioRxiv* 1–6 (2020). doi:10.1101/2020.04.23.051870

46. Mirzakhalili, E., Barra, B., Capogrosso, M. & Lempka, S. F. Biophysics of Temporal Interference Stimulation. *Cell Syst.* **11**, 557-572.e5 (2020).

47. von Conta, J. *et al.* Benchmarking the effects of transcranial temporal interference stimulation (tTIS) in humans. *Cortex* **154**, 299–310 (2022).

48. Ma, R. *et al.* High Gamma and Beta Temporal Interference Stimulation in the Human Motor Cortex Improves Motor Functions. *Front. Neurosci.* **15**, 1–11 (2022).

49. Hutcheon, B. & Yarom, Y. Resonance, oscillation and the intrinsic frequency preferences of neurons. *Trends Neurosci.* **23**, 216–222 (2000).

50. Acerbo, E. *et al.* Focal Non-invasive Deep-brain Stimulation with Temporal Interference for the Suppression of Epileptic Biomarkers. 1–21 (2022).

51. Wessel, M. J. *et al.* LTP-like noninvasive striatal brain stimulation enhances striatal activity and motor skill learning in humans. *bioRxiv* 1–30 (2022). doi:10.1101/2022.10.28.514204

52. Violante, I. R. *et al.* Non-invasive temporal interference electrical stimulation of the human hippocampus. (2022).

53. Abe, M. *et al.* Reward improves long-term retention of a motor memory through induction of offline memory gains. *Curr. Biol.* **21**, 557–562 (2011).

54. Steel, A., Silson, E. H., Stagg, C. J. & Baker, C. I. The impact of reward and punishment on skill learning depends on task demands. *Sci. Rep.* **6**, 1–9 (2016).

55. Vassiliadis, P., Lete, A., Duque, J. & Derosiere, G. Reward timing matters in motor learning. *iScience* (2022).

56. Izawa, J. & Shadmehr, R. Learning from sensory and reward prediction errors during motor adaptation. *PLoS Comput. Biol.* **7**, 1–12 (2011).

57. Mawase, F., Uehara, S., Bastian, A. J. & Celnik, P. Motor Learning Enhances Use-Dependent Plasticity. *J. Neurosci.* **37**, 2673–2685 (2017).

58. Iacono, M. I. *et al.* MIDA: A multimodal imaging-based detailed anatomical model of the human head and neck. *PLoS One* **10**, (2015).

59. Krause, M. R., Vieira, P. G., Csorba, B. A., Pilly, P. K. & Pack, C. C. Transcranial alternating current stimulation entrains single-neuron activity in the primate brain. *Proc. Natl. Acad. Sci. U. S. A.* **116**, 5747–5755 (2019).

60. Krause, M. R., Vieira, P. G., Thivierge, J. P. & Pack, C. C. Brain stimulation competes with ongoing oscillations for control of spike timing in the primate brain. *PLoS Biol.* **20**, 1–27 (2022).

61. Johnson, L. *et al.* Dose-dependent effects of transcranial alternating current stimulation on spike timing in awake nonhuman primates. *Sci. Adv.* **6**, 1–9 (2020).

62. Antal, A. & Herrmann, C. S. Transcranial Alternating Current and Random Noise Stimulation: Possible Mechanisms. *Neural Plast.* **2016**, (2016).

63. Alekseichuk, I., Wischnewski, M. & Opitz, A. A minimum effective dose for (transcranial) alternating current stimulation. *Brain Stimul.* **15**, 1221–1222 (2022).

1226 64. Jiang, T. Brainnetome: A new -ome to understand the brain and its disorders.
1227 *Neuroimage* **80**, 263–272 (2013).

1228 65. Areshenkoff, C. N., de Brouwer, A. J., Gale, D. J., Nashed, J. Y. & Gallivan, J. P.
1229 SEPARATE AND SHARED LOW - DIMENSIONAL NEURAL ARCHITECTURES
1230 FOR ERROR - BASED AND REINFORCEMENT. (2022).
1231 doi:10.1101/2022.08.16.504134

1232 66. Floyer-Lea, A. & Matthews, P. M. Changing brain networks for visuomotor control
1233 with increased movement automaticity. *J. Neurophysiol.* **92**, 2405–2412 (2004).

1234 67. Floyer-Lea, A. & Matthews, P. M. Distinguishable brain activation networks for
1235 short- and long-term motor skill learning. *J. Neurophysiol.* **94**, 512–518 (2005).

1236 68. Graybiel, A. M. & Grafton, S. T. The striatum: Where skills and habits meet. *Cold*
1237 *Spring Harb. Perspect. Biol.* **7**, 1–14 (2015).

1238 69. McLaren, D. G., Ries, M. L., Xu, G. & Johnson, S. C. A generalized form of
1239 context-dependent psychophysiological interactions (gPPI): A comparison to
1240 standard approaches. *Neuroimage* **61**, 1277–1286 (2012).

1241 70. Codol, O., Holland, P. J., Manohar, S. G. & Galea, J. M. Reward-Based
1242 Improvements in Motor Control Are Driven by Multiple Error-Reducing
1243 Mechanisms. *J. Neurosci.* **40**, 3604–3620 (2020).

1244 71. Sidarta, A., Vahdat, S., Bernardi, N. F. & Ostry, D. J. Somatic and reinforcement-
1245 based plasticity in the initial stages of human motor learning. *J. Neurosci.* **36**,
1246 11682–11692 (2016).

1247 72. Shirer, W. R., Ryali, S., Rykhlevskaia, E., Menon, V. & Greicius, M. D. Decoding

subject-driven cognitive states with whole-brain connectivity patterns. *Cereb. Cortex* **22**, 158–165 (2012).

73. Morishita, T. & Hummel, F. C. Non-invasive Brain Stimulation (NIBS) in Motor Recovery After Stroke: Concepts to Increase Efficacy. *Curr. Behav. Neurosci. Reports* **4**, 280–289 (2017).

74. Donnelly, N. A. *et al.* Oscillatory activity in the medial prefrontal cortex and nucleus accumbens correlates with impulsivity and reward outcome. *PLoS One* **9**, 14–17 (2014).

75. Schall, T. A., Wright, W. J. & Dong, Y. Nucleus accumbens fast-spiking interneurons in motivational and addictive behaviors. *Mol. Psychiatry* **26**, 234–246 (2021).

76. Pisansky, M. T. *et al.* Nucleus Accumbens Fast-Spiking Interneurons Constrain Impulsive Action. *Biol. Psychiatry* **86**, 836–847 (2019).

77. Kirby, K. N., Petry, N. M. & Bickel, W. K. Heroin addicts have higher discount rates for delayed rewards than non-drug-using controls. *J. Exp. Psychol. Gen.* **128**, 78–87 (1999).

78. Mitchell, J. M., Fields, H. L., D'Esposito, M. & Boettiger, C. A. Impulsive responding in alcoholics. *Alcohol. Clin. Exp. Res.* **29**, 2158–2169 (2005).

79. Catanese, J., Carmichael, J. E. & van der Meer, M. A. A. Low- and high-gamma oscillations deviate in opposite directions from zero-phase synchrony in the limbic corticostriatal loop. *J. Neurophysiol.* **116**, 5–17 (2016).

80. Rothé, M., Quilodran, R., Sallet, J. & Procyk, E. Coordination of high gamma

activity in anterior cingulate and lateral prefrontal cortical areas during adaptation. *J. Neurosci.* **31**, 11110–11117 (2011).

81. Del Arco, A., Park, J., Wood, J., Kim, Y. & Moghaddam, B. Adaptive encoding of outcome prediction by prefrontal cortex ensembles supports behavioral flexibility. *J. Neurosci.* **37**, 8363–8373 (2017).

82. Yoshimoto, A., Shibata, Y., Kudara, M., Ikegaya, Y. & Matsumoto, N. Enhancement of Motor Cortical Gamma Oscillations and Sniffing Activity by Medial Forebrain Bundle Stimulation Precedes Locomotion. *eNeuro* **9**, 1–14 (2022).

83. Courtemanche, R., Fujii, N. & Graybiel, A. M. Synchronous, Focally Modulated β-Band Oscillations Characterize Local Field Potential Activity in the Striatum of Awake Behaving Monkeys. *J. Neurosci.* **23**, 11741–11752 (2003).

84. Costa, R. M. *et al.* Rapid Alterations in Corticostriatal Ensemble Coordination during Acute Dopamine-Dependent Motor Dysfunction. *Neuron* **52**, 359–369 (2006).

85. Engel, A. K. & Fries, P. Beta-band oscillations-signalling the status quo? *Curr. Opin. Neurobiol.* **20**, 156–165 (2010).

86. Uehara, S., Mawase, F. & Celnik, P. Learning similar actions by reinforcement or sensory-prediction errors rely on distinct physiological mechanisms. *Cereb. Cortex* **28**, 3478–3490 (2018).

87. Mathis, M. W., Mathis, A. & Uchida, N. Somatosensory Cortex Plays an Essential Role in Forelimb Motor Adaptation in Mice. *Neuron* **93**, 1493-1503.e6 (2017).

88. Brücke, C. *et al.* Scaling of movement is related to pallidal γ oscillations in patients with dystonia. *J. Neurosci.* **32**, 1008–1019 (2012).

89. Soderstrom, N. C. & Bjork, R. A. Learning Versus Performance: An Integrative Review. *Perspect. Psychol. Sci.* **10**, 176–199 (2015).

90. Dhawale, A. K., Miyamoto, Y. R., Smith, M. A. & Ölveczky, B. P. Adaptive Regulation of Motor Variability. *Curr. Biol.* **29**, 3551-3562.e7 (2019).

91. Beliaeva, V., Savvateev, I., Zerbi, V. & Polania, R. Toward integrative approaches to study the causal role of neural oscillations via transcranial electrical stimulation. *Nat. Commun.* **12**, 1–12 (2021).

92. Krakauer, J. W., Hadjiosif, A. M., Xu, J., Wong, A. L. & Haith, A. M. Motor Learning. **9**, 613–663 (2019).

93. Averbeck, B. & O'Doherty, J. P. Reinforcement-learning in fronto-striatal circuits. *Neuropsychopharmacology* **47**, 147–162 (2022).

94. Acerbo, E. *et al.* Focal non-invasive deep-brain stimulation with temporal interference for the suppression of epileptic biomarkers. *Front. Neurosci.* **16**, 1–12 (2022).

95. Oldfield, R. C. The assessment and analysis of handedness: The Edinburgh inventory. *Neuropsychologia* **9**, 97–113 (1971).

96. Kaplan, B. A. *et al.* Automating Scoring of Delay Discounting for the 21- and 27-Item Monetary Choice Questionnaires. *Behav. Anal.* **39**, 293–304 (2016).

97. Mitchell, M. R. & Potenza, M. N. Recent Insights into the Neurobiology of Impulsivity. *Curr. Addict. Reports* **1**, 309–319 (2014).

1314 98. Brainard, D. H. The Psychophysics Toolbox. *Spat. Vis.* **10**, 433–436 (1997).

1315 99. Pelli, D. G. The VideoToolbox software for visual psychophysics: transforming
1316 numbers into movies. *Spat. Vis.* **10**, 437–442 (1997).

1317 100. Dayan, E., Averbeck, B. B., Richmond, B. J. & Cohen, L. G. Stochastic
1318 reinforcement benefits skill acquisition. *Learn. Mem.* **21**, 140–142 (2014).

1319 101. Grossman, N. Modulation without surgical intervention. *Science (80-.).* **361**, 461–
1320 462 (2018).

1321 102. Antal, A. *et al.* Low intensity transcranial electric stimulation: Safety, ethical, legal
1322 regulatory and application guidelines. *Clin. Neurophysiol.* **128**, 1774–1809 (2017).

1323 103. Ekhtiari, H. *et al.* A checklist for assessing the methodological quality of concurrent
1324 tES-fMRI studies (ContES checklist): a consensus study and statement. *Nat.*
1325 *Protoc.* **17**, 596–617 (2022).

1326 104. Bossetti, C. A., Birdno, M. J. & Grill, W. M. Analysis of the quasi-static
1327 approximation for calculating potentials generated by neural stimulation. *J. Neural*
1328 *Eng.* **5**, 44–53 (2008).

1329 105. Hasgall, P. *et al.* "IT'IS Database for thermal and electromagnetic parameters of
1330 biological tissues," Version 4.1. (2022). doi:10.13099/VIP21000-04-1

1331 106. Seeck, M. *et al.* The standardized EEG electrode array of the IFCN. *Clin.*
1332 *Neurophysiol.* **128**, 2070–2077 (2017).

1333 107. Bates, D., Mächler, M., Bolker, B. M. & Walker, S. C. Fitting linear mixed-effects
1334 models using lme4. *J. Stat. Softw.* **67**, (2015).

1335 108. Ryu, E. Effects of skewness and kurtosis on normal-theory based maximum

likelihood test statistic in multilevel structural equation modeling. *Behav. Res. Methods* **43**, 1066–1074 (2011).

109. Nieuwenhuis, R., te Grotenhuis, M. & Pelzer, B. Influence.ME: Tools for detecting influential data in mixed effects models. *R J.* **4**, 38–47 (2012).

110. Luke, S. G. Evaluating significance in linear mixed-effects models in R. *Behav. Res. Methods* **49**, 1494–1502 (2017).

111. Searle, S. R., Speed, F. M. & Milliken, G. A. Population marginal means in the linear model: An alternative to least squares means. *Am. Stat.* **34**, 216–221 (1980).

112. Ben-Shachar, M., Lüdecke, D. & Makowski, D. effectsize: Estimation of Effect Size Indices and Standardized Parameters. *J. Open Source Softw.* **5**, 2815 (2020).

113. Derosière, G., Billot, M., Ward, E. T. & Perrey, S. Adaptations of motor neural structures' activity to lapses in attention. *Cereb. Cortex* **25**, 66–74 (2015).

114. Okamoto, M. *et al.* Three-dimensional probabilistic anatomical cranio-cerebral correlation via the international 10-20 system oriented for transcranial functional brain mapping. *Neuroimage* **21**, 99–111 (2004).

115. Rolls, E. T., Huang, C. C., Lin, C. P., Feng, J. & Joliot, M. Automated anatomical labelling atlas 3. *Neuroimage* **206**, 116189 (2020).

116. Hampton, W. H., Alm, K. H., Venkatraman, V., Nugiel, T. & Olson, I. R. Dissociable frontostriatal white matter connectivity underlies reward and motor impulsivity. *Neuroimage* **150**, 336–343 (2017).

117. Mosley, P. E. *et al.* The structural connectivity of discrete networks underlies

impulsivity and gambling in Parkinson's disease. *Brain* **142**, 3917–3935 (2019).

118. Ma, I. *et al.* Ventral striatal hyperconnectivity during rewarded interference control in adolescents with ADHD. *Cortex* **82**, 225–236 (2016).

119. Wang, Q. *et al.* Dissociated neural substrates underlying impulsive choice and impulsive action. *Neuroimage* **134**, 540–549 (2016).